Green synthesis of Europium (III) Oxide nanoparticles using *Hibiscus sabdariffa* flower extract

By

Zamavezi Kweyama

(201151099)

Submitted in fulfilment of the academic requirements for degree of Master of Science in the Department of Physics and Engineering, University of Zululand, KwaDlangezwa.

Supervisor: Prof. Malik Maaza (NRF/ iThemba LABS)

Co-Supervisors: Dr. Betty Kibirige (University of Zululand)

Dr. Ntevheleni Thovhogi (NRF/iThemba LABS)

February 2018

DECLARATION

I hereby declare that Synthesis of Europium (III) Oxide (Eu_2O_3) nanoparticles using *Hibiscus sabdariffa* flower extract ; physical & optical properties is my original work and has not been submitted in any form to University or Institution. Credit has been given where use of others is made.

Z Kweyama February 2018

DEDICATION

This thesis is dedicated to my parents Mr Malusi Christian Kweyama, Nonhlanhla Beauty Kweyama and my siblings Sthembile Mandisa Bele, Mthunzi Clement Kweyama, Sandile Kweyama, Lungani Kweyama and Siyabonga Kweyama for the encouragement and support.

ACKNOWLEDGEMENTS

I would like thank the Lord almighty for the strength, patience and for making this work a success.

I am very grateful to the following people and organization without whose assistance, advice and guidance this thesis would not have been possible.

My deep and sincere gratitude goes to my supervisor Professor Malik Maaza (NRF-iThemba LABS and UNESCO-UNISA African chair in nanoscience and nanotechnology) for allocating me this fascinating research topic. Your excellent supervision, guidance, motivation and constant support throughout this work is deeply appreciated.

I appreciate the guidance of my co-supervisor Dr Ntevheleni Thovhogi (NRF-iThemba LABS) for her constant encouragement and interest in my progress. Thank you for your patience and teaching me the laboratory routines. Without Dr Thovhogi encouragements and support I would not have been able to come this far or to this moment.

I am very thankful to Dr Betty Kibirige my co-supervisor (University of Zululand) for her great patience, useful suggestions and execution of the thesis work. Thank you for your continuous help towards registration and every process you went through at Unizulu for my project to be registered and your guidance throughout my course. I owe a sincere thanks to Dr Nolubabalo Matinise (NRF-iThemba LABS). Thank you for the laboratory skills and analysis of results skills you taught me. Thank you for always being ready when I needed help and for all possible solution to every problem I was facing. I benefited much from her.

I would also like to thank Dr Saleh Khamlich (NRF-iThemba LABS) for his constant guidance during my course work, making sure that there is progress in my project. And also for his assistance with the UV-Vis and fluorescence techniques.

To my UNESCO fellow colleagues and the Material Research Department staff members; your guidance, support and contribution were vital for the success of this project. I am grateful for their support and help rendered. I would like to thank all the people who contributed in any way for the successful completion of this project. Last but not least, University of Zululand, National Research Foundation (NRF), iThemba LABS, the

UNESCO-UNISA African chair in Nanoscience and Nanotechnology for financial support during this study; I am really grateful.

LIST OF ABBREVIATIONS

NPs: Nanoparticles

EuO: Europium (II) oxide

Eu_2O_3: Europium (III) oxide

Eu_3O_4: Trieuropium tetroxide

$EuN_3O_9.5H_2O$: Europium nitrate penta-hydrate

HB: *Hibiscus sabdariffa*

SEM: Scanning Electron Microscopy

HRTEM: High Resolution Transmission Electron Microscopy

EDS: Electron Dispersive X-rays Spectroscopy

XRD: X-Rays Diffraction

FT-IR: Fourier Transform Infrared Spectroscopy

UV-Vis-NIR: Ultraviolet and visible spectrometer

PL: Photoluminescence

CV: Cyclic Voltammetry

EIS: Electrochemical Impendence Spectroscopy

EPD: Electrophoretic Deposition

XPS: X-ray Photoelectron Spectroscopy

CVD: Chemical Vapour Deposition

PEC: Photo-electrochemical

TOPO: Trioctly phosphine

CNTs: Carbon nanotubes

EISA: Evaporation Induced Self-assembly process

DI-H_2O: Deionized water

UV: Ultra-Violet

IR: Infrared

LIST OF SYMBOLS

hv: Photo energy

A: Material constant

Eg: Energy band gap

n: Numeric constant

θ: Bragg angle

a_o: Lattice constant

h, k, l: Miller indices

β: Quartz standard

ABSTRACT

Nowadays there is a need to develop eco-friendly processes, inexpensive and nontoxic chemical use in the synthesis protocol in order to obtain biocompatible and harmless nanoparticles. Green chemistry approach is the eco-friendly process which has taken the researchers attention globally due to its advantages over conventional methods. This ecological method has potential in transforming the inorganic metal ions into metal oxides NPs via the bio-reduction of molecules present in the particular organism.

This contribution reports on the synthesis, the main physical and optical properties of Europium (III) oxide (Eu_2O_3) nanocrystals synthesized for the first time by a completely green physical-chemistry process using *Hibiscus sabdariffa* (HB) natural flower extract and Europium nitrate pentahydrate ($Eu(NO_3)_3.5H_2O$) salts as a precursor. The HB natural extract solution was used as a reducing agent for the production of Eu_2O_3 nanoparticles. The 1 g of $EuN_3O_9.5H_2O$ was dissolve in 100 ml of HB extract solution. The precipitate obtained was dried in the oven set at 100^oC and thereafter annealed for 2 hrs at various temperature; 300^oC, 500^oC and 700^oC using a standard furnace. The structural and optical properties of such biosynthesis nanocrystals were analyzed using High Resolution Transmission Electron Microscopy (HRTEM), Scanning Electron Microscopy (SEM), Electron Dispersive X-rays Spectroscopy (EDS), X-Ray Diffraction (XRD), Fourier Transform Infrared Spectroscopy (FT-IR), Raman Spectroscopy, Ultraviolet and visible spectrometer (UV-Vis-NIR) as well as room temperature photoluminescence (PL). The HRTEM and SEM results showed the images of small NPs formed, which indicated that the Eu_2O_3 NPs are nano-scaled with a mixed population of crystalline particles. The TEM and XRD analysis showed grain size of nanoparticles ranging between 14 nm and 25 nm. The XRD results confirmed the characteristic body centered cubic (BCC) structure of Eu_2O_3 nanoparticles and the UV-Vis proved that Eu_2O_3 absorbs in a wide range of electromagnetic wave from ultraviolet region. The luminescence properties of such cubic were characterized by an intense red emission centered at 614.93 nm ($^5D_0$-$^7F_2$). It was observed that a biosynthesized cubic Eu_2O_3 nanocrystal is an efficient luminescence material due to a very good luminescent response with potential application as red phosphors.

These results represent an important step forward in the investigation of Eu_2O_3 nanoparticles properties synthesized via green chemistry process. It is a promising cost-effective path and energy wise non-consuming with zero waste end products for highly stable and well-characterized nanoparticles. The green synthesized Eu_2O_3 nanoparticles would be beneficial for the development of nontoxic, clean and environmentally friendly biosynthesis procedure.

KEY WORDS

Green chemistry

Hibiscus sabdariffa

Natural extract

Europium (III) oxide (Eu_2O_3)

Nanoparticles

Rare earth oxides

Photoluminescence

TABLE OF CONTENTS

TABLE OF FIGURES

LIST OF TABLES

THESIS OUTLINE

Chapter one: Introduction

This chapter provides the background of the study, the need of green chemistry approach to synthesize metal oxides NPs. The chapter also includes the review and the importance of green chemistry processes. The problem statement, aims and objectives of the study are also included in this chapter.

Chapter two: Literature review

This section provides literature on Eu_2O_3 NPs. Its structural and optical properties arising from their 4f transitions which make them useful in a variety of applications such as laser materials, phosphors, catalyst and up-conversion are also described. The literature on the synthetic methods used and the approach used in the current work to synthesize NPs is also given in this chapter.

Chapter three: Experimental procedure

This section covers the materials and methods used throughout the synthesis process of the NPs. It also provides the information on the characterization techniques used in this work.

Chapter four: Results and discussion

This section highlights the results obtained from each characterization technique. It also provides information on the surface morphology, elemental analysis, crystallographic structure, chemical bonding, vibration spectroscopy and photoluminescence studies of the NPs.

Chapter five: Conclusions

This section gives the brief summary and conclusions of the research study and the future work.

CHAPTER ONE: INTRODUCTION

1.1. Background of the study

Materials with nano-size particles exist in nature. Metal oxide nanoparticles (NPs) are nano-size metals within the range of 1 to 100 nm in one dimension. There are divided into four main categories nanoparticles (0D), nanowires and rods (1D), sheets and platelets (2D) and nanostructures (3D) [1]. Nanomaterials research have attracted large number of research scientists and is still growing rapidly due to their interesting properties of nanomaterials and their potential applications. These applications have advantages in areas such as mechanics, optics, biomedical sciences, chemical industry, electronics, drug delivery and photo electrochemical application [2].

Metal oxides play a very important role in many areas of chemistry, physics, and material science, they are able to form large diversity of oxides compounds with the number of structural geometries which can show metallic, semiconductor or insulator character [3]. The oxides of rare earth elements are known for their excellent mechanical, chemical, thermal, optical and dielectric properties. They are the most desired luminescent materials due to their transition within 4f electron shell. These oxides have a number of structural phases known as A-type hexagonal, B-type monoclinic and C-type cubic phase. These are in order of C→B→A when the temperature is increased up to ~2000^{o}C. Above 2000^{o}C new phases are formed called H for hexagonal and X for cubic [3-4, 12]. Europium (III) Oxide (Eu_2O_3) known as dieuropium trioxide is a semiconductor metal oxide with the band gap (Eg) of 4.5 eV to 4.0 eV in UV light region using equation;

$$(\alpha hv)^2 = A(hv - Eg) \qquad (1)$$

where *hv* is the photo energy, α is the absorption coefficient and *A* is the constant for the material. It appears in the form of a pinkish white powder; non-toxic when comparing to other heavy metal oxides [4].

NPs have a surprising long history, they are not necessarily produced by modern synthesis laboratories [5] some of them are naturally occurring namely organic and inorganic NPs which are produced by weathering, wildfires and microbial processes. Where organic includes carbon NPs while inorganic includes magnetic NPs, noble metal oxides and semiconductor NPs (Zinc oxide, Europium oxide) [5-6]. The history of NPs started when nanostructures were formed in the early meteorites, however, the scientific production of nanomaterials began very late. By 1857, Michael Faraday was the first person to report the colloidal gold particles. In the early 1940's, the precipitated and fumed silica NPs were being produced for ultrafine carbon black for rubber reinforcements. In the 1960's and 1970's metallic nanoproducts were produced for magnetic records tapes [7,8-9]. In 1976 nanocrystals were obtained by inert gas evaporation technique [9].

Today nanostructures engineering expands in a rapidly growing number of structural and functional materials, both organic and inorganic [7]. Their production has become broad and interdisciplinary area of research and development activity globally where physical and chemical methods are used. Such methods include facile electrodeposition, sol-gel techniques, gas phase condensation, colloidal precipitation router, microwave-assisted surface chemistry, solvothermal, ultrasonication, hydrothermal and a pulsed laser ablation synthesis and biological (green chemistry) methods though green chemistry is still a developing technique [2]. Most of these methods are expensive and potentially hazardous to the environment and living organisms. Green chemistry includes bacteria, yeast, fungi, and plants etc. This approach is generally a cost-effective path and is energy wise non-consuming with zero waste end products [4,9-10]. Thus, the present research is devoted to the possibility of metal oxide nanoparticles synthesis using plant extracts.

Recently NPs production using Green chemistry (plant extracts) is among the most interesting in the field of science, they are able to reduce metal ions faster than other organisms to metal atoms.

So far NPs produced using plant extracts have been used in some practical applications. For example, silver NPs produced using *tridax procumbens* extract similar to one obtained by physical or chemical technique has been used for strong antimicrobial activity against *ascherichia coli*. Silver NPs produced using cluster bean extracts were recently used as a biosensor to determine ammonial, agriculture and biomedicine application [11]. Platinum NPs obtained using holy basil extract used for catalytic activity and for hydrogen fuel elements [11].

1.2. Problem statement

Nanotechnology is an important field that is rapidly growing in the scientific field of producing and constructing devices and also an important area of the research concentrating on the synthesis of NPs with different sizes, morphology and chemical composition in material science receiving global attention due to it interesting applications. Metal oxide NPs are being increasingly used as commercial products in many sector of the economy. More recent uses of nanotechnology mean more and more engineered NPs produced by these several physical and chemical approaches which are complex, costly, requiring vacuum condition, consuming a great amount of energy, requiring a lot of time to produce stable ones and they generate harmful waste based precursors [6, 12-13]. These man- made NPs enter our atmosphere, soil and water environment which affects the human health and the environment at large.

Nowadays there is a growing need to develop eco-friendly processes, inexpensive and also which do not use toxic chemicals in the synthesis protocol in order to obtain biocompatible and harmless Eu_2O_3 NPs. Green chemistry approach is an eco-friendly process which has taken the researchers attention globally due to its advantages over conventional methods and can be used as an economic and valuable alternative for large scale-production of NPs [2,12]. This eco-friendly method has potential in transforming the inorganic metal ions into metal oxide NPs via the bioreduction of molecules present in the particular organism [6, 12]. This study therefore reports on the synthesis of Eu_2O_3 nanoparticles by completely green physical-chemistry process using *Hibiscus sabdariffa* flower natural extract as an effective reducing agent.

1.3. Aim of the study

The aim of this study was to produce Europium (III) oxide (Eu_2O_3) nanoparticles via *hibiscus sabdariffa flower* extract and to investigate its optical and physical properties.

1.3.1. Main objectives

- To investigate the effects of annealing at different temperatures (300, 500, &700 ^{o}C) on the biosynthesized Eu_2O_3 NPs.
- To investigate the physical and optical properties of biosynthesized Eu_2O_3 NPs using various techniques (e.g. X-ray diffraction (XRD), Transmission electron microscopy (TEM) measurements and other techniques).
- To investigate the photoluminescence properties of the synthesized Eu_2O_3 NPs and it response as phosphor application.

1.4. References

1. D. Mirela, ‘Metallic nanoparticles’, university of Nova Gorica, slideshare.
2. S. Iravani, ‘Green synthesis of metal nanoparticles using plants’, Green chemistry, vol. 13, 2638-2650 (2011).
3. M. Fernandez-Gacia, J.A. Rodriguez, Metal oxide, Department of chemistry, brookhaven National Laboratories, (2007).
4. C. Zeng, K. Zheng, X. Meng, Z.Yan, Z. Ye, R. Su, S. Zhong ,X. Meng, Z.Yan, Z. Ye, R. Su, S. Zhong, ‘Synthesis of porous europium oxide particles for photoelectrochemical water splitting’, Electrochimica Acta, vol. 165, 396-401 (2015).
5. F. J. Heiligtag, M. Niederberger, ‘The fascination world of nanoparticles research’, Materials today, vol 16, (2010).
6. M. Singh, S. Manikhadan, A. K. Kumaraguru, ‘Nanoparticles: A new technology with wide applications’, Journal of nanoscience and nanotechnology, (2010).
7. C. E. Tabor, ‘Some optical and catalytic properties of metal nanoparticles, school of chemistry and biochemistry’, Georgia, Institute of Technology, December (2009).
8. A. Alagarasi, ‘Introduction to nanomaterials’.
9. T. S. Spreeprasad, T Pradeep, ‘Noble metal nanoparticles book’.
10. N. Bala, S. Saha, M. Chakraborty, M. Maiti, S. Das, R. Basu, P. Nandy, ‘Green synthesis of zinc oxide nanoparticles using *Hibiscus sabdariffa leaf* extract: effect of temperature on the synthesis, anti-bacterial activity and anti-diabetic activity’, Royal society of chemistry, vol. 5, 4993-5003 (2015).
11. D. Philip, ‘Green synthesis of gold and silver nanoparticles using *hibiscus rosa sinensis’*, Physica E: Low-dimensional Systems and nanostructures, vol. 42, 1417-1424 (2010).
12. V.V Makarov, A.J. Love, O.V Sinitsyna, S.S Makarova,I.V. Yaminsky, M.E. Taliansky, N.O. Kalinina, ‘Green nanotechnologies: Synthesis of metal nanoparticles using plants’, Acta naturae, vol 20, 35-43 (2014).
13. N. Thovhogi, A. Diallo, A. Gurib-Fakim, M. Maaza, ‘Nanoparticles green synthesis by *Hibiscus sabdariffa flower* extract: Main physical properties’ , Journal of alloys and compounds, vol. 647, 392-396 (2015).
14. www.nanocap.eu.

CHAPTER TWO: LITERATURE REVIEW OF Eu_2O_3 NPs

2.1. Structural properties

Europium oxide is divided into three different forms in which the element can exist as EuO, Eu_2O_3 and Eu_3O_4. They are all the allotropes of europium oxide with different crystal structures and variety of magnetic characteristics considering ferromagnetic for EuO, anti-ferromagnetic for Eu_3O_4 and paramagnetic for Eu_2O_3 [1]. Among them Eu_2O_3 is one of the excellent candidate material due to its extensive mechanical, chemical, thermal, optical and dielectric properties. Europium (III) oxide (Eu_2O_3) also known as dieuropium trioxide or europia [2, 4] is a rare earth stable sesquioxide chemical of the Eu^{3+} ion with two common crystal structures which are monoclinic B-Type (mS30, space group=C2/m, No.12) and cubic C-Type structure (cI80, space group=Ia-3, No.206) [3-6] where C-Type structure matches with manganese (III) oxide shown below in **Fig. 2.1 (a)** and (**b**). Europium oxidizes and reacts with air at 150-180°C to form Eu_2O_3, [3-5, 8].

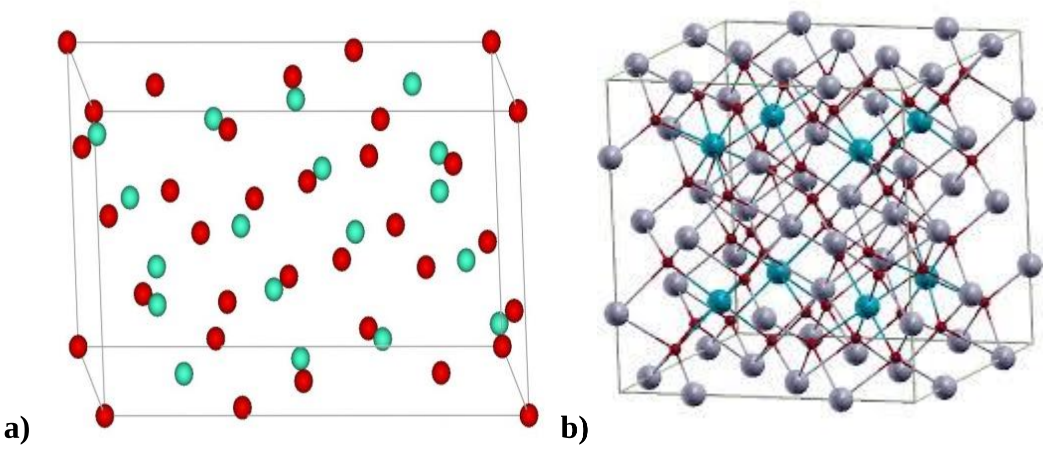

Figure 2.1: The structures of Europium (III) Oxide **(a)** B-Type crystal structure where red atoms are oxygen and green atoms are Europium, **(b)** C-Type crystal structure where red atoms represent oxygen [3-4].

Accordingly, over past few years a variety Eu_2O_3 nanostructure were synthesized and investigated successfully by relatively expensive and toxic approach. Such porous Europium oxide particles for photo-electrochemical water splitting has been obtained by the electrochemical synthesis, microspheres and nanoparticle-wires by hexamethylene tetramine (>90°C) provides OH^- and intrinsic anisotropy [6-8]. The nanocrystalline thin films were synthesized by electrophoretic deposition (EPD) [6-8], pulsed laser deposited Fe doped

Eu_2O_3 thin film produced via laser ablation [9], europium oxide nanolayer coated on the titanium by sol-gel [10], Eu_2O_3 NPs by the simple microwave-assisted surface chemistry [9] as well as Eu_2O_3 nanorods by hydrothermal method [12] etc. The synthesis of nano-scaled Eu_2O_3 engineered by Green chemistry process has been reported by Diallo et al. [13]. The properties of Eu_2O_3 nanomaterials are dependent on the crystallinity, crystalline size, crystallographic orientation and morphology respectively. Eu_2O_3 nanomaterials with controllable size and architecture are very desirable. In order to convert as-prepared particles, the annealing process needs to be performed in air for a specific time. After annealing, the colour of Eu_2O_3 NPs changes from brownish to white and the SEM images exhibit particle size expansion and more homogeneity [6]. From the crystallographic viewpoint, Eu_2O_3 belong to the Bravais lattice with the space group Ia-3 and unit cell lattice bulk parameters $a_{bulk} = b_{bulk} = c_{bulk} = 10.868$ Å. Most literature has reported that the identification of the crystalline phase of nanomaterials before and after calcination is performed only by x-ray diffraction (XRD). All the peaks can be well indexed to the body-centered cubic with the lattice constant a=10.86 Å corresponding to (JCPDS 65-3182), where by the narrow peaks and strong peaks indicate good crystallinity of Eu_2O_3 NPs [6-7, 13]. Eu_2O_3 in its body-centred cubic phase has a unit cell that is made of 16 molecules with 24 Eu^{3+} ion on sites with $C3_{3i}$ (S6) symmetry [11-12].

2.2. Optical Properties

Semiconductor metal oxides such as Eu_2O_3 have good properties, making them attractive materials. Eu_2O_3 has extensive electronic, optical and chemical characteristics coming from it well-defined transition 4f electrons. The optical properties are red emission at 612 nm, long fluorescence lifetime and spectrally narrow [13-14]. The pH of Eu_2O_3 is estimated to be 5.5 to 6. It is insoluble in water but easily dissolve in acid during chemical reaction which results in the loss of optical properties in nanoparticles. Direct coating with silica can be used as a cap on the surface of the particles to prevent europium oxide from losing its optical properties [9, 15]. The purity of rare earth metal oxide available is 99.9 to 99.99% [12] and its melting point is 2.350ºC, its apparent density is 7.40 g/cm^3 and it is hydroscopic, [2]. Eu_2O_3 is also a photoactive material for photocatalytic degradation of organic pollutants [15] and other properties like its dispersivity, size and crystal structure which can be determined by X-ray diffraction (XRD), transmission electron microscopy (TEM), scanning electron microscopy

(SEM), energy dispersive X-ray spectrometry (EDS), and Fourier-transform infrared spectrometry (FT-IR) at a room temperature.

Rare earth oxides have been widely used as high performance luminescence devices because of it interesting characteristics from their 4f electron. Eu_2O_3 major emission bands of Eu^{3+} is usually centred or allocated at the peak of 612 nm peak (red) due to it well defined transition within the 4d-4f electron shell [11] and the force electric dipole transition $^5D_0$- $^7F_2$ shown in the **Figure2.2 below**. This major peak indicate the cubic phase product [17], which is the one of the three primary colours (red, blue, green) from which a wide white spectrum can be generated by appropriate mixing [18] and it is widely used in many applications. The wavelength of Eu^{3+} f-f transition within emission $^5D_0$- $^7F_2$ depends on the material and the colour of the material is determined by the wavelength of light that is absorbed [18]. Absorption occurs because the electrons are induced by the photons of the incident light to make the transition between wavelengths. Eu_2O_3 is a very important oxide phosphor primarily because oxide phosphors exhibit improved stability in high vacuum environments and under low voltage electron bombardment it shows high resistance. The wide band gap (Eg) of a semiconductor nanomaterial was estimated to around 4.0 eV according to the equation 1 mentioned earlier in page 1 by Zeng et al. [6]. C- type cubic Eu_2O_3 is estimated to have approximately 22 Raman active modes namely 4Ag, 4Eg and 14 Fg, which are connected to the stretching vibrations [11].

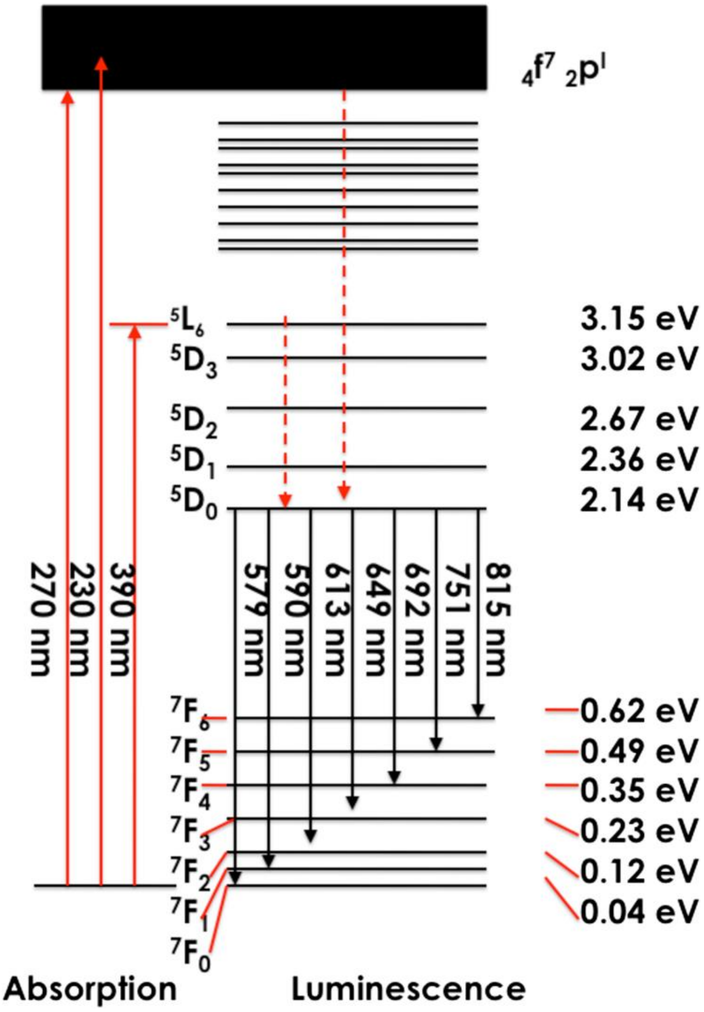

Figure 2.2: The energy level diagram of the optical transitions of Eu^{3+} ion and various emission transitions.

2.3. Synthesis methods of nanoparticles

Nanomaterials are synthesized by assembling atoms/ molecules together. Basically there are two approaches to NPs synthesis; the bottom up and the top down approach. Bottom up approach is making small stuff bigger, a molecule or simple salt that has right atoms is taken and a chemical reaction performed to build the nanoparticles atom by atom. Top-Down approach involves breaking a large material into nanoparticles. A large material is taken and drill mechanically to process it into tiny nano-sized pieces [19]. The bottom-up approach includes supercritical fluid synthesis, spinning, plasma of flame spraying synthesis, green synthesis, sol-process & sol-gel process, laser pyrolysis, eurosol based, chemical vapour deposition (CVD) and atomic or molecular condensation [19-20]. The top-down approach consists of mechanical milling, etching (chemical), electro-explosion, sputtering and laser ablation (thermal) [20]. Previously NPs were synthesized only by physical (sputtering, solvothermal etc) and chemical methods (sol-gel, reduction etc) techniques, which both fall under bottom-up and top-down approaches. Bottom-up approach is receiving interest globally because the fabrication is much less expensive than the top-down approach and it starts with an atom or molecule to build the nanostructure. These physical and chemical processes are costly, potentially harmful to the environment and living organism; they bring new environmental problem effects which results in the need for new methods to synthesize NPs [21]. So in the research of cheaper and nontoxic pathways for NPs synthesis, scientist have used microorganisms and plant extracts for synthesis. The use of Biological Method has become actively pursued as an alternative, efficient, inexpensive and eco-friendly method for producing NPs [19, 21].

2.3.1. Physical and chemical process

Eu_2O_3 NPs can be prepared through various physical and chemical methods. F-doped Tin (IV) Oxide (SnO_2) glass substrate and facile electrodeposition methods and thermal treatment can be used to prepare Eu_2O_3 particles as a photo anode for photo-electrochemical (PEC) water splitting applying chemical reaction to separate water from oxygen and hydrogen [15]. Nanocrystalline material can be successfully prepared or demonstrated by the number of processes such as sol-gel techniques, gas phase condensation and colloidal precipitation [15-19] router between 2-40 nm [15]. In the colloidal approach the reaction occur at a room temperature with the measured solution added in methanol with equal amount of trioctly phosphine (TOPO) solution, which has the number of desirable functions towards nanocrystal [13, 16].

(Feng and his co-worker) used a simple microwave-assisted surface chemistry to synthesize the inorganic phosphor nanoparticles of Eu_2O_3. These nanoparticles were being used as fluorescence dye in biology because of it excellent sensitivity in an immunoassay for atrazine, where atrazine is used to check the presence of $Eu_2O_{3,}$ [9]. The approach of carbon nanotubes (CNTs) as removable template in facile solvothermal is used for preparing europium oxide nanotubes and nanowires which has a number of successful application. During the preparation of Eu_2O_3 nanotubes the calcination temperature used is between 350-850 ºC, while for nanowires is between 850-1050 ºC. The characteristics for nanotube and nanowire depends on the temperature; when the thermal temperature is >1050 ºC the nanowires become less than a micrometre and nanotubes show amorphous characteristics when the temperature is < 350 ºC [14]. Besides the solvothermal method, several methods can be used to synthesize Eu_2O_3 nanowires such as ultrasonication, hydrothermal and sol-gel methods which uses porous anodic alumina as a template.

Optical properties including high photoluminescence efficiency and pure emission colour which have a good impact in luminescence material are found only in rare earth europium. Pulsed laser ablation by novel method is also used for the preparation of nanoeuropium oxide. In this process, the laser beam focuses on the target of europium oxide with required diameter while ethanol flows over the target under a nitrogen atmosphere [22]. **Table 2.1** below shows different methods that have been used to synthesize the Eu_2O_3 nanoparticles.

Table 2.1: Synthesis of Europium oxide nanoparticles using other Methods.

Method of synthesis	**Shape (Morphology)**	**Size (nm)**	**References**
Vacuum evaporation	Spheres	20.6	Dakhel et al. (2002)
Sonochemical synthesis	Spheres	5-10	Pol et al. (2002)
Electrophoretic deposition (EPD) process	Spheres	4.0	Mahajan et al. (2006)
Evaporation-induced self-assembly (EISA) process	Quasi-spherical	9.5	Castro et al. (2007)
Pulsed laser ablation	Spherical	20	Qian-huo et al. (2008)
Simple solution phase reaction	Spherical	1.0 – 3.0	Kattel et al. (2012)
Green process	Spheres	16.5 ± 0.25	Diallo et al. (2016)

2.3.2. Green chemistry process

Nanostructures with different shapes including nanoparticles, nanowires, nanorods, and nanocrystalline materials have been prepared using main methods known as physical and chemical processes. Such methods include facile electrodeposition, sol-gel techniques, gas phase condensation, colloidal precipitation router, microwave-assisted surface chemistry, solvothermal, ultrasonication, hydrothermal and a pulsed laser ablation synthesis. However most of these methods are expensive and potentially hazardous to the environment and living organisms [9, 13, 15-16]. A technological approach to prevent and to eliminate the use of toxic chemicals has been researched lately and this is known as Green chemistry process.

Green chemistry process for synthesis of metal oxide nanoparticles (NPs) has become a major focus for researchers and industries producing NPs. Various nanomaterials such as ZnO, CeO_2, Ag, Au etc. have been synthesized successfully by green process using various plants materials such as *Hibiscus Sabdariffa* (HB) [23-24]. Green process is an alternative sustainable technology whereby plant is extracted for NPs production via Bio reduction process. The main aim of this method is to reduce or eliminates the use and generation of hazardous substances. This approach has been used because it is easy, cost-effective, environmentally safe, biocompatible, non-toxic and also soluble in water [21, 23].

Plant extracts are a very promising tool for preparing NPs via green route and they are used as reducing/capping agent without using inorganic or organic solvents but mix with the metal salts during the bio-reduction process [24]. For example, Silver NPs have been successfully prepared by *Iresine Herbstii* (Herbst's blood leaf), *Eurobia Nivilia* (leaf milk hedge) and *Nerium Olender*. Platinum NPs have been prepared by *Ocinum Sanctum* extract [21] and these metal oxide NPs have a number of desirable applications. **Table 2.2** below show several plants that have been used for efficient and rapid synthesis of different nanoparticles.

Table 2.2: Green synthesis of other metal oxide nanoparticles using plants**.**

Plant	**Nanoparticles produced**	**Shape (Morphology)**	**Size (nm)**	**References**
Capsicum annuum L.	Au	Spherical	10 ± 2	Li et al. (2007)
Seaweed (Sargassum muticum)	Fe3O4	Cubic	18 ± 4	Mahnaz et al. (2013)
Gum karay	CuO	Spherical	7.8 ± 2.3 4.8 ± 1.6	Thekkae Padil et al. (2013)
Aspalathuslinearis	ZnO	Quasi-spherical	4.08± 0.08	Diallo et al. (2015)
Agathosmabetulina	CdO	Quasi-spherical	8	Thema et al. (2015)
Hibiscus sabdariffa	CeO_2	Spheres	3.9	Thovhogi et al. (2015)

2.3.2.1. Plant material: *Hibiscus sabdariffa*

Figure 2.3: A picture of the *Hibiscus sabdariffa* flowers, **(A)** showing fresh flower and **(B)** dried flowers [commons.wikimedia.org/wiki/File:Flower_Hibiscus_Sabdariffa.jpg].

Hibiscus Sabdariffa (HB) belongs to Malvaceae family **(fig.2.3)** and it is also known as Indian Sorrel. It originates from West Africa and grows in tropical and subtropical regions. It has red flowers and it contain proteins, fats, carbohydrates, acids, minerals, vitamins as well as phenolic compounds. Stem, root and leaves are the important part of the plant where phytochemical compounds are located [23, 25]. HB has the number of effective applications such as herbal medicine (helps to lower fever, hypertension, and treat cancer), beverages (herb tea, juices), food (flavours and colouring) and vegetables [21-22]. Thovhogi et al. successfully synthesized the highly crystallize single phase CeO_2 NPs using natural extract of HB without adding any toxic substances [24]. Some of the biomolecules present in HB extracts are similar to the one found in other plants such as *Aspalatus Linearis* as shown in **fig.2.4** this includes phenolic compounds and phenolic acid such as nitric acid, hydroxytric acid and hibiscus acid. Flavonoids such as quercetin, luteolin and gossipetin with their glycosides and anthocyanin are found in calyces such as cyaniding-3-glucoside, delphinidin-3-glucoside, cyaniding-3-sambubioside and delphinidin-3-sambubioside [21, 23, 25]. Bala et al. reported on the highly soluble and stable ZnO NPs synthesized from HB leave extracts, and its use as an antibacterial and antidiabetic agent [25].

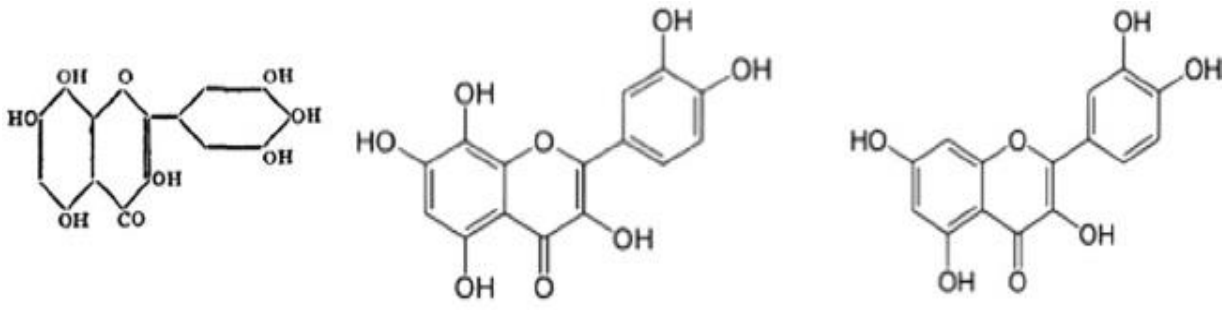

Hibiscetin

Gossypetine

Quercetin

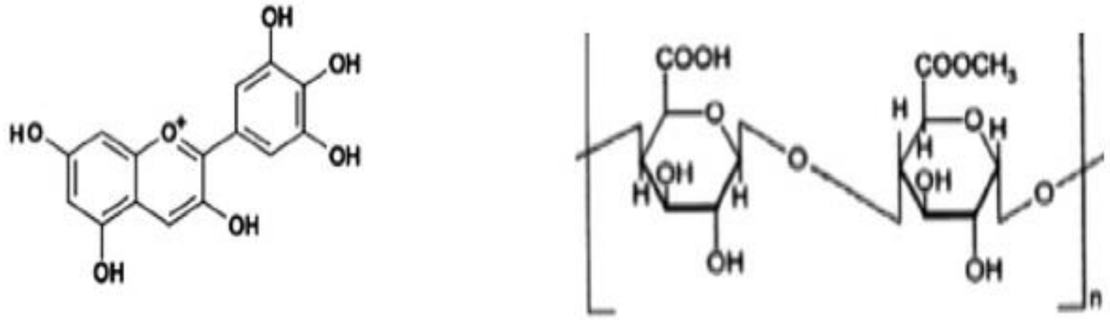

Delphinidin

Pectin

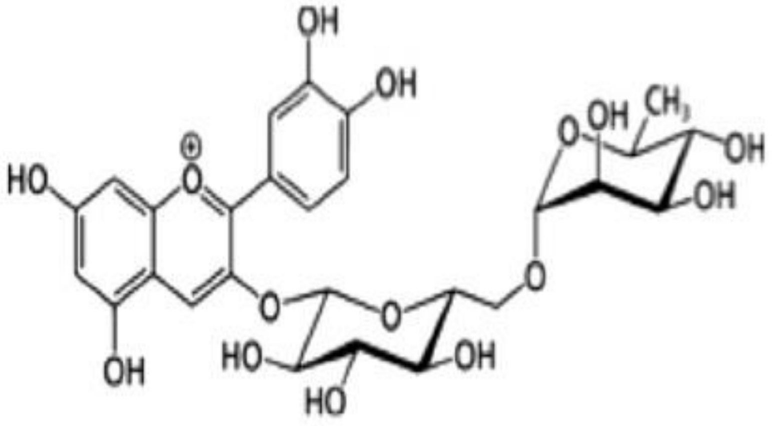

Cyanidin 3- sambubioside

Figure 2.4: Biomolecule compounds within *Hibiscus Sabdariffa* extracts [24].

2.4. Plant extraction and Biosynthesis of oxide NPs.

Most reviewed literature shows that the solvent used to extract dye from the plant in order to synthesize NPs is de-ionized water, the natural plant as the environmental safety reducing agent and the nontoxic metal salts material for stabilizing NPs. Philip et al, successfully prepared gold and silver NPs using *hibiscus rosa sinensis* extracts where 200 ml of de-ionized water was added to 2 g of HB leaf at 300 K for 1 min and filtered to obtain the solution extract. The obtained solution was used as a reducing metabolites and stabilizing agent for NPs [10]. In addition, Sone et al. biosynthesized Sm_2O_3 NPs via *Callistemon viminalis'* natural extract [28], and Thema et al. synthesize Monteponite CdO NPs by *agathosma betulina* natural extract [27], while Bala et al. synthesized zinc oxide NPs using HB leaves extracts using green chemistry process [25]. This lead to, Thovhogi et al. biosynthesizing CeO_2 NPs using HB flower extract [24].

In brief, 400 ml of distilled water in a beaker was mixed with 10 grams of clean HB and kept at room temperature for 2 hours while stirring. The whatman filter papers were used to remove unwanted solid materials from the extracted solution. The filtered material was then mixed with the aqueous solution of $Ce(NO_3)_36H_2O$ and heated for a specified time, centrifuged, oven dried and annealed at higher temperature which was 500 ^oC to obtain the desired NPs of CeO_2 [23]. So far this is the only procedure used to synthesize NPs by green process using various plants materials. For the experimental procedure in this study, the same protocol reported by Thovhogi et al. is followed to synthesize the Europium oxide nanoparticles from *Hibiscus sabdariffa* flower extracts using green chemistry procedure.

Most reviewed literature reveal that the crystallinity of the sample increases with the increase in the temperature and when the sample is dried at lower temperature it exhibit no characteristic of absorption band, shows amorphous features but when it dried at high temperature approximately above 60 ºC, it results in sharp surface Plasmon resonance showing the presence of NPs. When the temperature is increased the bioactive molecules absorb on the surface of the particle and they can also be lost when it is increased too much [24]. NPs are successfully formed at a room temperature; the rising of the temperature affect the structure of the sample. It was reported in the literature that the pH of the solution used has a major impact on the size of the NPs rather than the shape and that the material become accessible at a very acidic pH. Hence, when the pH decreases, large NPs are produced, while small NPs are produced at higher pH. The rate of formation of the NPs is found to be slower when the concentration is lower [20-21, 24].

2.5. Applications of Eu_2O_3

Eu_2O_3 has a number of applications including red or blue phosphor in television, fluorescent lamps, production of fluorescent glass, anti-counterfeiting phosphors in euro banknotes and also known as a great neutron absorber which is used in nuclear control rods [1, 14]. Rare earth metal oxides are precise transitions within 4f electrons which making it an attractive material with desirable applications such as light emitters [13], used in high throughput essay for environment monitoring, molecular labels for sensitive detection of proteins and nuclei acid in immunoassay [9]. Since Eu_2O_3 major emission band is centred about 612 nm on a primary colour due to its well defined transitions within 4f electrons shell, its usage in phosphors and luminescent devices is significant [15]. It is also used in laser material nanometre scale optoelectronic devices [14] and in up-conversion material, low voltage cathodoluminescent devices and catalyst. This material is known as a good photo anode for water splitting and also used in photocatalytic degradation of organic pollutants since it is an efficient photoactive anode. And Mahajan et al also prepared Eu_2O_3 thin films via electrophoretic deposition (EPD) which yielded translucent and opaque thin films. These thin films had a marked anisotropy to the size and distribution of the constituents of microstructure. These Eu_2O_3 thin films were used in nanoscale applications such as photoactive coatings, optical data storage and fluorescent video displays [6].

2.6. References

1. D. Lee, J. Seo, L. Valladares, O.A. Quispe, H.W. Barnes, ‘Magnetic and structural properties of yellow europium oxide compound and $Eu(OH)_3$’, Journal of solid state chemistry, vol. 228, 141-145 (2015).
2. N. Dilawar, S. Mehrotra, ‘A Raman spectroscopic study of C-type rare earth sesquioxides’, Material characterization, vol. 59, 462-467 (2008).
3. en.wikipedia.org/wiki/Europium(III)oxide.
4. en.wikipedia.org/wiki/Europium.
5. S.C. Atkinson, ‘Crystal structures and phase transitions in the rare earth oxides’, School of computing, science and engineering, (2013).
6. C. Zeng, K. Lou, X. Meng, Z. Yan, Z. Ye, ‘Synthesis of Porous Europium Oxide Particles for Photo-electrochemical Water Splitting’, Electrochimica Acta, vol. 165, 396-401 (2015).
7. Y. Li, M. Ge, J. Li, J. Wang, H. Zhang, ‘Synthesis of mesoporous Eu_2O_3 microspheres and Eu_2O_3 nanoparticle-wires as well as their optical properties’, Society of chemistry, vol. 13, 637-641 (2011).
8. S.V Mahajan, D.W Kavich, M.L Redigolo, J.H Dickerson, ‘Structural properties of electrophoretically deposited europium oxide nanocrystalline thin films’, Journal of material science, vol. 41, 8160-8165 (2006).
9. S. Kumar, R. Prakash, R.J Choudhary, D.M Phase, ‘Structural, XPS and magnetic studies of pulsed laser deposited Fe doped Eu_2O_3 thin films’, Material research bulletin, vol. 70, 392-396 (2015).
10. V.G Pol, R. Reisfeld, A. Gedanken, ‘Sonochemical Synthesis and optical properties of europium oxide nanolayer coated on titania’, Chemical Material, vol. 14, 3920- 3924 (2002).
11. J. Feng, G. Shan, A. Maquieira, M. E. Koivumen, ‘Fuctionalized Europium oxide nanoparticles used as fluorescent label in an immunoassay for atrazine’, Analytical Chemistry, vol. 75, 5282-5286 (2003).
12. J. Kang, Y. Jun, B. Min and Y. Sohn, ‘Full characterization of $Eu(OH)_3$ and Eu_2O_3 nanorods’, Applied Surface Science, vol. 314, 158-165 (2014).
13. A. Diallo, B.M. Mothudi, E. manikandan, M. Maaza, ‘Luminescent Eu_2O_3 nanocrystals by aspalatus linearis extract: structural and optical properties’,Journal of nanophotonics, vol. 10(2), (2016).

14. L. Tucker, F. Karney, P. McMilan, S. Lin, L. lyring, ‘Raman and resonance raman spectroscopy of selected rare-earth sesquioxides’, Applied Spectroscopy, vol. 38, 857 (1984).

15. G. Wakefield, H.A. Keron, P.J. Dobson, J.L. Hutchison, ‘Synthesis and properties of sub-50nm europium oxide nanoparticle’, Journal of colloid and interface science, vol. 215, 179-182 (1999).

16. H. Yang, D. Zhang, L. Shi, J. Fang, ‘Synthesis and strong red photoluminescence of europium oxide nanotubes and nanowires using carbon nanotubes as templates’, Acta materialia, vol. 56, 955-967 (2008).

17. C. Zeng, K. Zheng, X. Meng, Z.Yan, Z. Ye, R. Su, S. Zhong , X. Meng, Z.Yan, Z. Ye, R. Su, S. Zhong, ‘Synthesis of porous europium oxide particles for photo-electrochemical water splitting’, Electrochimica Acta, vol. 165, 396-401 (2015).

18. R. Bazzi, M.A. lores, C. Louis, K. Lebbou, W. Zhang, C. Dujardin, S. Roux, B. Mercier, G. Ledoux, E. Bernstein, P. Perriat, O. Tillement, ‘Synthesis and properties of europium-base phosphors on the nanometer scale:Eu2O3, Gd2O3:Eu and Y2O3’, Journal of colloid and interface science, vol. 273, 191-197 (2004).

19. D.Y. Medina, S. Orozco, I. Hernandez, R.T. Hernandez, C. Falcony, ‘Characterization of europium lanthanum oxide film prepared by spray pyrolysis’, Journal of non-crystalline solids, vol. 357, 3740-3743 (2011).

20. M. Singh, S. Manikhadan, A. K. Kumaraguru, ‘Nanoparticles: A new technology with wide applications’, Journal of nanoscience and nanotechnology, (2010)

21. S. Iravani, ‘Green synthesis of metal nanoparticles using plants’, Green chemistry, vol. 13, 2638-2650 (2011).

22. V.V Makarov, A.J. Love, O.V Sinitsyna, S.S Makarova,I.V. Yaminsky, M.E. Taliansky, N.O. Kalinina, ‘Green nanotechnologies: Synthesis of metal nanoparticles using plants’, Acta naturae, vol. 6 No.1 (20), 35-43 (2014).

23. W. Zhang, Y. Zhang, J. Tang, Y. Zhang, L. Wang, Q. Ling, ‘Study on preparation and optic properties of nano europium oxide-ethanol sol by pulsed laser ablation’, Thin solid films, vol. 417, 43-46 (2002).

24. N. Thovhogi, A. Diallo, A. Gurib-Fakim, M. Maaza , ‘Nanoparticles green synthesis by *Hibiscus sabdariffa flower* extract: Main physical properties’, Journal of alloys and compounds, vol. 647, 392-396 (2015).

25. N. Bala, S. Saha, M. Chakraborty, M. Maiti, S. Das, R. Basu, P. Nandy, ‘Green synthesis of zinc oxide nanoparticles using *Hibiscus sabdariffa leaf* extract: effect of temperature on the synthesis, anti-bacterial activity and anti-diabetic activity', Royal society of chemistry, vol. 5, 4993-5003 (2015).

26. I. Borras-Linares, S. Fernandez-Arroyo, D. Arraez-Roman, P.A. Palmeros-Suarez, R. Del, Val-Diaz, I. Andrade-Gonzales, A.Fernandez-Gutierrez, J.F. Gomez-Leyva, A. Segura-Carretero, 'Characterization of phenolic compounds ,anthocyanidin, antioxidant and antimicrobial activity of 25 varieties of Mexican Roselle (*Hibiscus sabdariffa*)', Industrial crops and products, vol. 69, 385-394 (2015).

27. A. Mungole and A. Chaturvedi, '*Hibiscus sabdariffa* L A rich source of secondary metabolites', International journal of pharmaceutical sciences review and research, vol. 6, 83-87 (2011).

28. F.T. Thema, P. Beukes, A. Gurib-Fakim, M. Maaza, 'Green synthesis of Monteponite CdO nanoparticles *by Agathosma betulina* natura extract', Journal of alloys and compound, vol. 646, 1043-1048 (2015).

29. B.T. Sone, E. Manikandan, A. Gurib-fakim, M. Maaza, 'Sm_2O_3 Nanoparticles green synthesis via callistemon viminals extract', Journal of alloys and compound, vol. 650, 357-362 (2015).

CHAPTER THREE: EXPERIMENTAL PROCEDURE AND CHARACTERIZATION TECHNIQUES

3. Experimental Section

3.1 Biosynthesis process

3.1.1 Materials used in the synthesis

An analytical grade reagent europium nitrate pentahydrate ($EuN_3O_9.5H_2O$), molecular weight 428.06 g/mol, 99.9 % purity trace metal basis together with petri dish were purchased from Sigma-Aldrich. The chemical reagent was used without further purification. Hibiscus sabdariffa flowers were used as chelating agent from West Africa. The distilled water (DI-H_2O) was used in all the synthesis process. The whatman filter papers from Lasec and oven to dry the precipitate from Guerre IK-interklimat. The furnace for annealing was purchased from Elite thermal synthesis.

3.1.2 Preparation of the plant extract

High quality dried flowers of *Hibiscus sabdariffa* (HB) were weighed **fig. 3.1** and initially cleaned thoroughly with cold water. In a typical setup 10 g of dried HB were submerged or mixed with 400 ml of distilled water (dH_2O) for 3 hours to extract the bioactive compounds from the HB at room temperature yielding a red coloured extract. The duration of 3 hours was considered to ensure the maximum extraction of the bioactive compounds from the HB flowers. The red solution was then filtered using whatman filter paper to remove unwanted solid materials. The extracted natural dye pH was ~2.54.

3.1.1 Synthesis of the europium oxide nanoparticles

Hibiscus sabdariffa flower extract was used to chelate europium-base salt. Analytical grade reagent $EuN_3O_9.5H_2O$ was used, 1 g of $EuN_3O_9.5H_2O$ in **fig.3.1** was dissolve in 100 ml of HB extract solution heated while stirring for 2 hrs and its pH was measured to be 1.73. The 1 g of $EuN_3O_9.5H_2O$ salt was considered to be the reasonable concentration to ensure the synthesis of Eu_2O_3 with maximum nanopowder. The precipitation obtained was then collected into a glass petri-dish and dried in the oven set at 100^oC. As the synthesized oxide based nanoparticles by green process are general amorphous, annealing is necessary to induce an effective crystallization and improve materials properties. The obtained precipitate was then annealed at various temperatures (300, 500 & 700 ^{o}C) for 2 hrs using standard furnace to observe the effect of temperature on the material and to remove bio-compounds in excess. The synthesis process was schematically presented in **fig 3.2**.

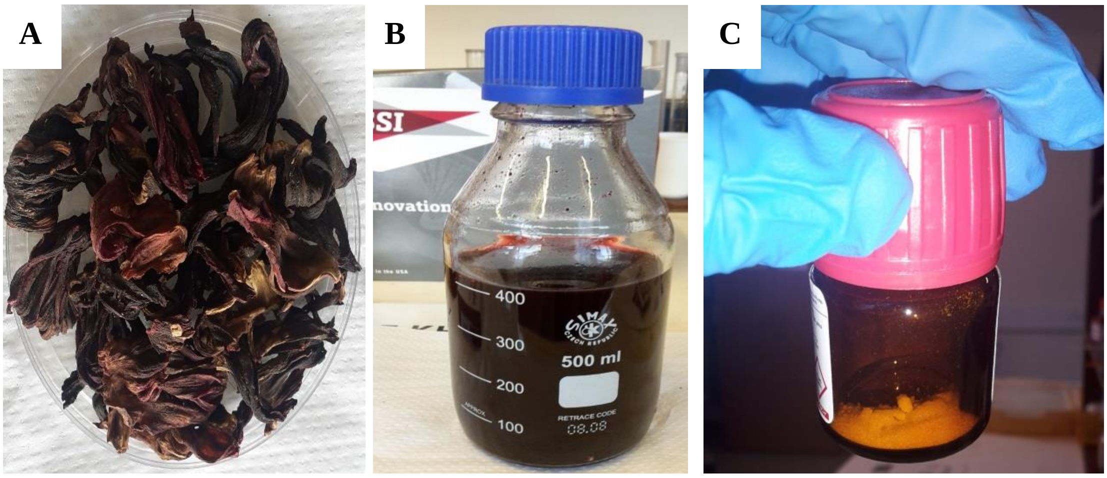

Figure 3.1: (A) Dried *Hibiscus sabdariffa* flowers, **(B)** extract that was mixed with the salt and **(C)** precursor ($EuN_3O_9.5H_2O$).

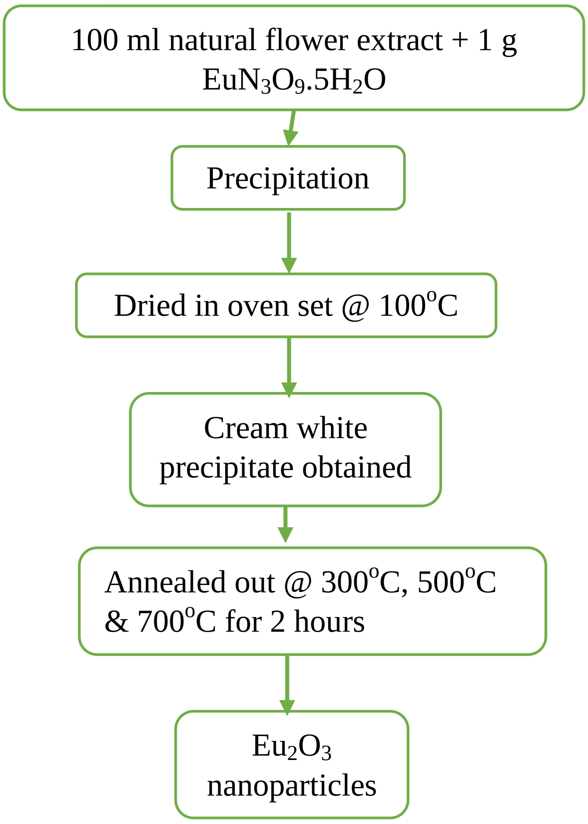

Figure 3.2: Schematic representation of the Eu_2O_3 production.

3.2. Material characterization

The main goal of the project was to synthesize Eu_2O_3 NPs and to investigate its optical properties, surface morphology, chemical composition and crystalline structure. The surface morphology, microstructure and the composition (element analysis) of the samples were analysed by scanning electron microscopy (SEM) and high resolution transmission electron microscopy (HRTEM) using FEI Tecna G2 Field Emission Gun operating 200 kV for sample confirmation. The chemical composition was determined by Energy X-ray dispersive spectroscopy and X-ray diffraction (XRD Bruker, D8 advanced with Cu Kα radiation, λ = 1.54060 Å), an analytical technique used to analyse the crystal structure and atomic spacing. FT-IR spectra was carried out using the pellets sample, prepared by mixing KBr (99.99%)-Fluka, Germany with the Eu_2O_3 nanopowder. Raman spectra were also recorded at room temperature using Raman spectrometer. The optical properties spectrum of Eu_2O_3 nanopowder (prior dissolved in ethanol) was measured in the range (200 – 800 nm) using UV-Vis-NIR spectrometer. Photoluminescence (PL) spectra of Eu_2O_3 nanoparticles were carried out in the range of (353 – 800nm) at a room temperature.

3.3. Characterizations techniques

After synthesizing Europium Oxide nanocrystals by a green chemistry process using *hibiscus sabdariffa* flower natural extract the main physical, optical properties were studied. The investigation and study of the nanopowder properties was conducted using different characterization techniques as described in **Table 3.1**.

Table 3.1: Analytical techniques to study Eu_2O_3 nanoparticles.

Characterization techniques	**Uses**
X-ray diffraction (XRD)	Phase identification of Eu_2O_3 nanoparticles
Scanning electron microscopy (SEM)	Surface morphology of Eu_2O_3 nanoparticles
Energy dispersive x-ray spectroscopy (EDS)	Elementary analysis Eu_2O_3 nanoparticles
High resolution transmission electron microscopy (HRTEM)	Particle size and morphology Eu_2O_3 nanoparticles
Fourier transform infrared spectroscopy (FT-IR)	Verify surface coating and chemical bonding of Eu_2O_3 nanoparticles
Raman	Vibrational properties of Eu_2O_3 nanoparticles
UV-visible	Verify bioactive compounds of Eu_2O_3 nanoparticles
Photoluminescence (PL)	Optical and electronic properties of Eu_2O_3 nanoparticles

3.3.1. Electron microscopy

3.3.1.1. Surface morphology characterization technique

An electron microscope is an instrument used to examine the very fine object such as nanometer (nm) to micrometer (μm) scale. It uses a beam of highly energetic electrons to examine the objects (to produce an image of variety of specimens). Detectors are used to collect the radiation and transform it into an image which carries more information about the topography, morphology and compounds that the object is composed of together with the crystallographic information [1-2]. This electron microscope displayed a highly improved magnification better than the optical microscopes that has limited resolution and magnification. The electron microscope was needed in the first place to get the light of microscope which had limitation, limited by the physics of light, magnification and resolution see the **Figure 3.2** below. The application of electron microscope can be useful in many fields such as biotechnology, biological science metallurgical. It is used in obtaining important information in nanoparticle research, pharmaceutical drug research, 3D structure visualization of viruses, proteins, single particles such as Ribosome tRNA, and lipids vesicles [2].

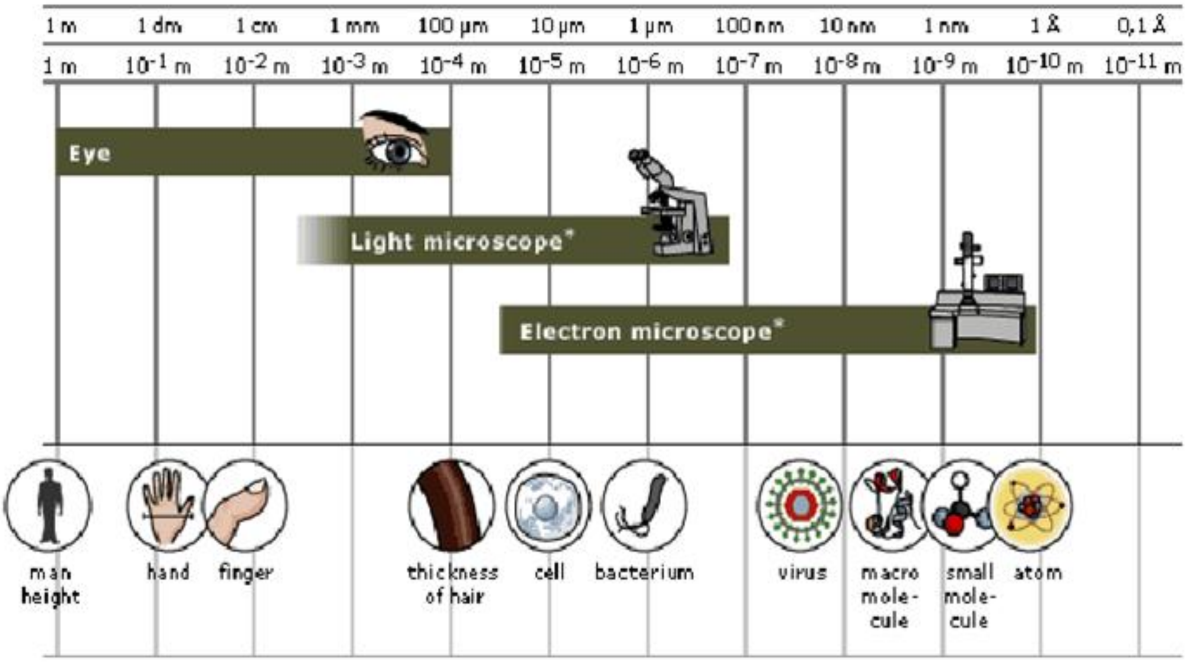

Figure 3.3: Diagram showing the comparison between light and electron microscope [3]

Table 3.2: Differences between optical and electron microscope

Optical microscope	**Electron microscope**
Low price	High price
Doesn't require vacuum for operation	Require vacuum for operation
Uses optical glass lens	Uses magnification lens
Have low magnification (500X & 1000X appx)	Have high magnification (10000X appx)
Small depth of field	Large depth of field

- **Two types of electron microscopes were used in this study:**
  Scanning Electron Microscopy (SEM) and Transmission Electron Microscopy (TEM)

3.3.1.1.1. Scanning Electron Microscope (SEM)

Description of the technique

SEM has 10x- 500 Kx magnification, 30 mm depth of field and 1.5 nm of resolution, which allows large amount of sample to be in focus at one time and produces an image that has a good representation of the three-dimensional sample [4]. It scans the sample with a high-energy beam of electrons focused in a vacuum into a fine probe that is rastered over the surface of the specimen (slides and the basics) generating primary backscattering, secondary electrons, X-rays and Auger electrons as shown in **Figure 3.3.**

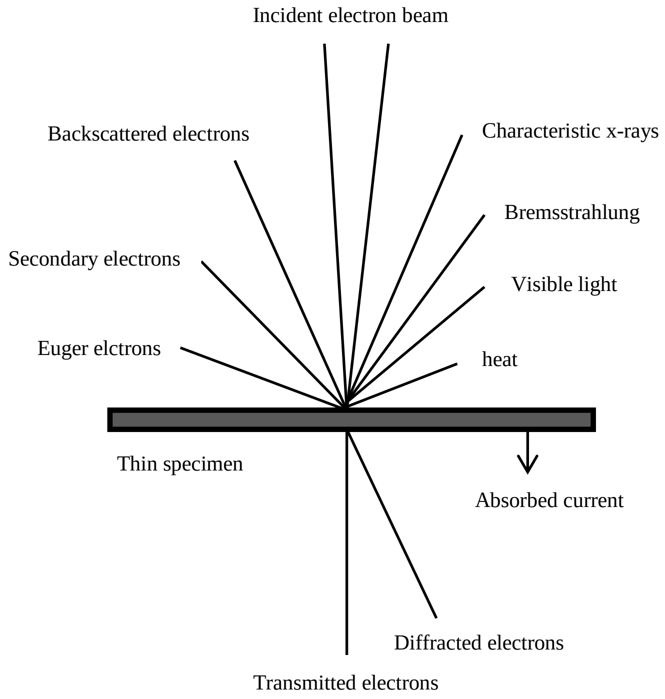

Figure 3.4: Demonstration of the interaction of incident electron beam with the sample and radiation signals generated during interaction [1].

Operation of the instrument

The scanning electron microscope uses magnetic lenses to direct the highly-energetic beam of electrons towards the direction of the specimen [1, 5]. Once the incident beam of electrons hits the surface of the specimen the electrons rapidly lose their speed and a strong interaction takes place at the surface of the specimen. This interaction produces a variety of radiation signals from the surface of the specimen as shown in **Figure 3.5** below. These radiation signals generated across the entire surface of the specimen are collected by a detector and an image is displayed on a screen [4-5].The final image provides data about the sample’s surface topography, morphology, crystallographic information, composition and other properties [6].

External view of SEM	Internal view of SEM
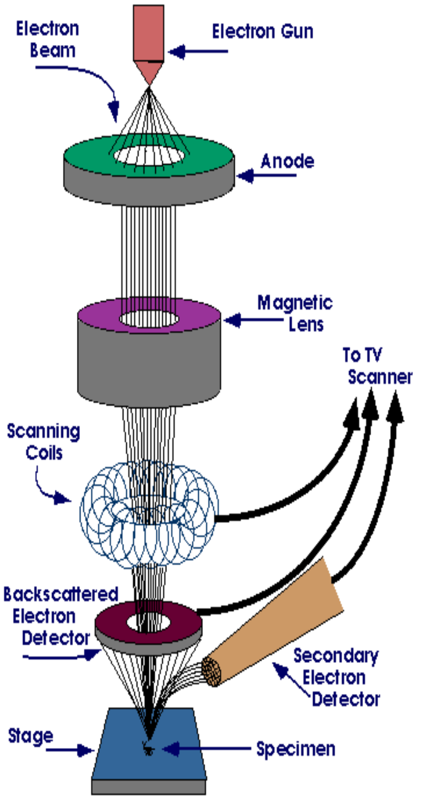	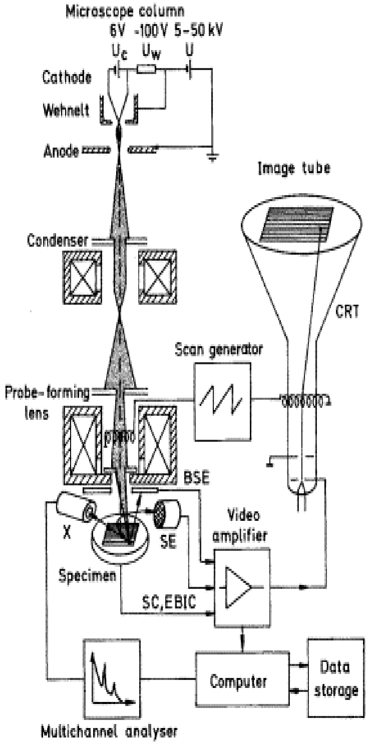

Figure 3.5: Schematic diagram showing the basic components of scanning electron microscope [3, 10].

Sample preparation

The Eu_2O_3 nanopowder was coated with argon and iridium using the sputter coater (Quorum Q 150 TES) to increase the conductivity of the sample. SEM and EDS were performed on the sample using Carl Zeiss Aunga Field Emission Scanning Electron Microscope (FEG SEM) imaging at 5 KeV. EDS was obtained with an OXFORD instrument X-MAX solid state silicon drift detector at 20 KeV.

3.3.1.1.2. High Resolution Transmission Electron Microscope (HRTEM)

Description of the technique

HRTEM is used to characterize materials, and can offer such a broad range of characterization with high spatial and analytical resolution. It is a central tool for complete characterization of nanoscale materials and devices [3]. HRTEM were developed because of the limited resolution in light microscopes which is imposed by the wavelength of visible light. It has a major role in biomaterials, bio/inorganic interfaces and nano-bio/biomaterial [3] and has major application in cancer research, virology, material science as well as pollution nanotechnology and semiconductor research.

Operation of the instrument

A beam of electrons interacts with a specimen to form an image. The HRTEM is similar to the light microscope except that it uses an electron beam rather than the light beam where by the brightness of the beam is controlled by the two condenser lenses and pass through the aperture to hit the sample surface [1,2]. The electrons after passing through the condenser lenses elastically scatter into the transmitted beam which pass through the objectives lenses and form the image display, the objective lenses and the selected area of the aperture that are used to choose the elastically scattered electrons that form the image of the microscope. After the electron beam has gone through all the 3 lenses, where by the first two controls the magnification of the image and the third is a projector lens which also controls the magnification and note how the size of the image changes. The formed image is shown either on fluorescent screen or on a monitor screen and printed as a photographic film.

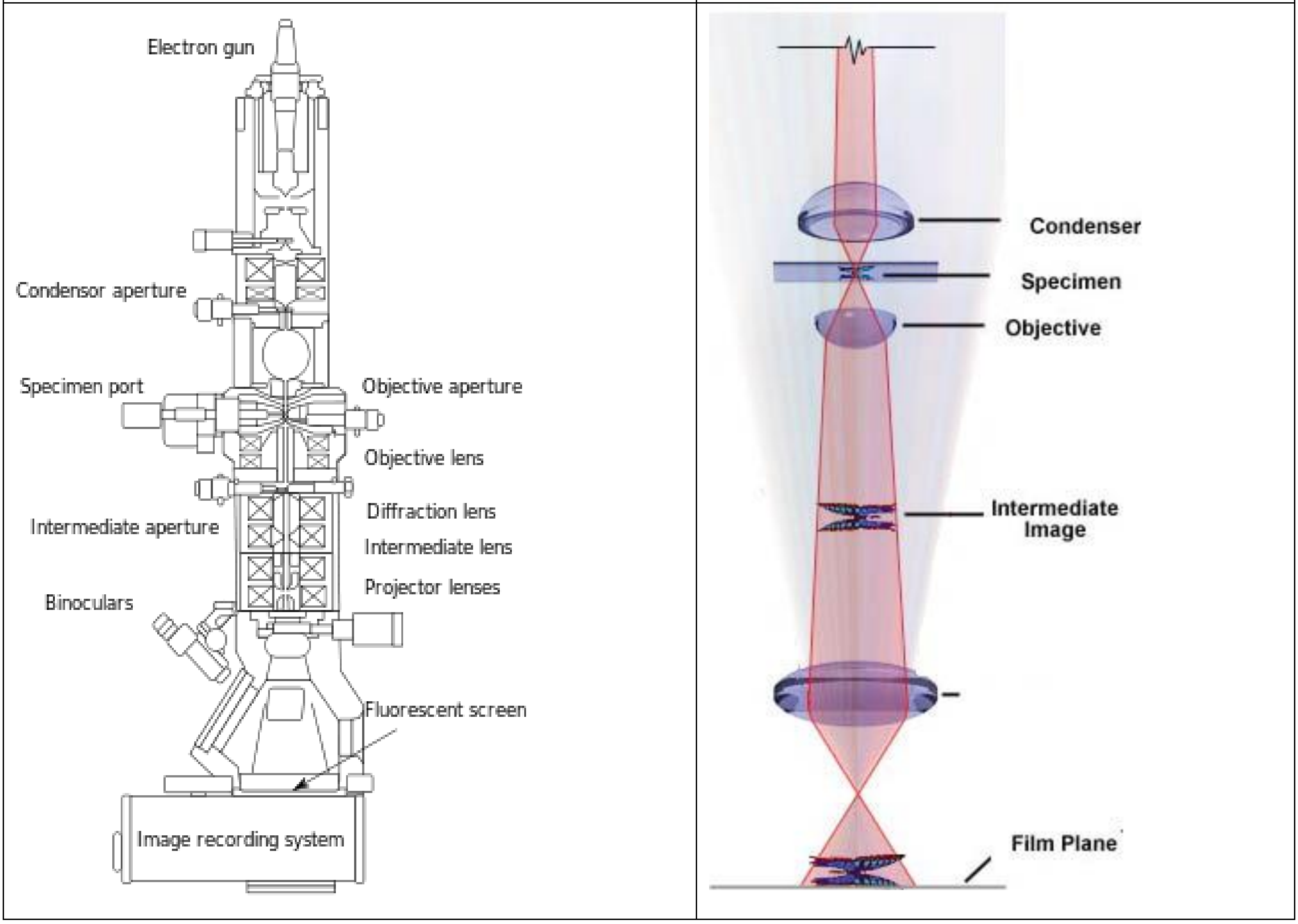

External view of TEM

Internal View of TEM

Figure 3.6: Schematic diagram showing the basic components of the transmission electron microscopy [2, 6].

Sample preparation

HRTEM analysis was performed using FEI Tecna G2 Field Emission Gun operating 200 kV. The samples were prepared by deposing small drops of dilute dispersion of Eu_2O_3 nanopowders ultrasonicated in acetone TEM grids. The grids were coated with a thin amorphous carbon support approximately ~20 nm since it has a low electron density. The samples were left for 10 minutes under a lamp light for them to be dry. The ultrasonication procedure of the solution of Eu_2O_3 nanopowder to acetone did not affect the chemical structure and the composition properties of the material. Thus, this samples were ready for TEM measurements.

Table 3.3: Comparison between scanning electron microscopy (SEM) and transmission electron microscopy (TEM) [3]

Scanning Electron Microscope (SEM)	**Transmission Electron Microscope (TEM)**
SEM is based on scattered electrons	TEM is based on transmitted electrons
No need in the SEM	Sample in TEM has to be cut thinner
Large amount of sample to be analysed	Only small amount of sample can be analysed
Used for surface, powders, polished and etched microstructures and chemical segregation	Used for imaging of dislocations, tiny precipitates, grain boundaries and other defects structures in solids
Smaller resolution	Much higher resolution

3.3.1.1.3. Energy Dispersive X-ray Spectroscopy (EDS)

Description of the technique

Energy dispersive X-ray spectroscopy (EDS) is a powerful technique which is connected to both SEM and TEM. For EDS measurements, the same procedure used for sample preparation for SEM has been used. It is widely used for exhibiting/ identifying what elements and chemical compounds present in the specific material. EDS has become a useful analytical tool in various areas such as materials science, nanotechnology, biology and microelectrons [11].

EDS is capable of identifying each and every element found in nanopowder. It consists of the characteristic x-rays produced when an incident beam of charged electrons or high energy electrons are directed a sample or specimen see **Figure 3.7.**

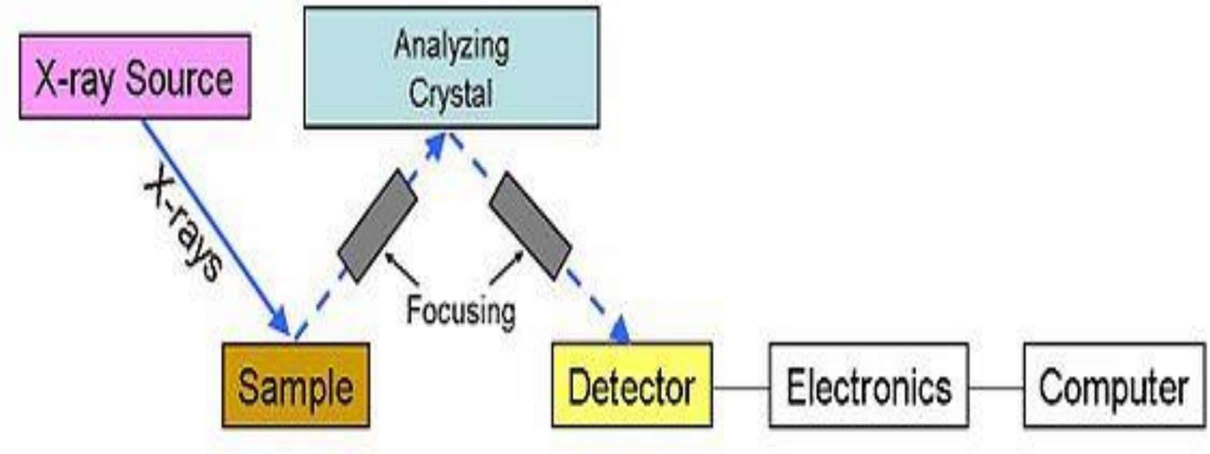

Figure 3.7: Components of an energy dispersive spectroscopy system [3].

Operation of the instrument

The X-rays are generated when the electron beam hits the sample. The x-rays formed escape the sample and hit the detector which creates a charge pulse in the detector, which is then converted into a voltage pulse with amplitude reflecting the energy of the detected x-ray. When the measurement is complete the voltage pulse will be converted to a digital signal, the x-ray spectrum **Figure 3.8,** is produced with the major peaks showing the elements present in the sample [11].

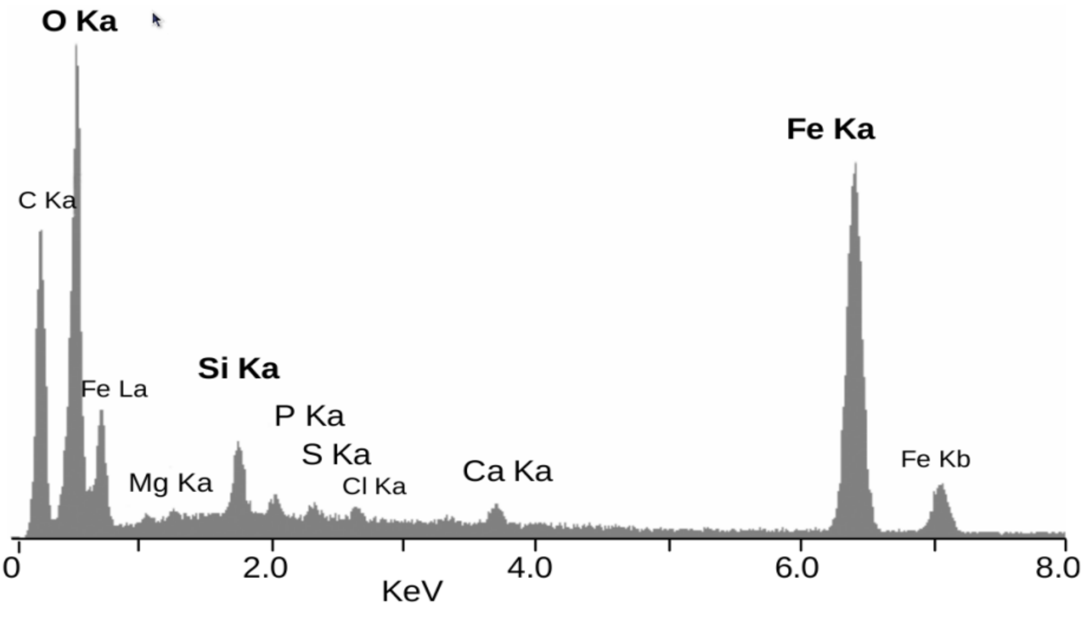

Figure 3.8: An energy-dispersive X-ray spectrum showing the main elements peaks [11].

Once the incident beam enters the sample it takes out the electrons from an inner shell (K-shell) see **Figure 3.9** and experience loss energy.

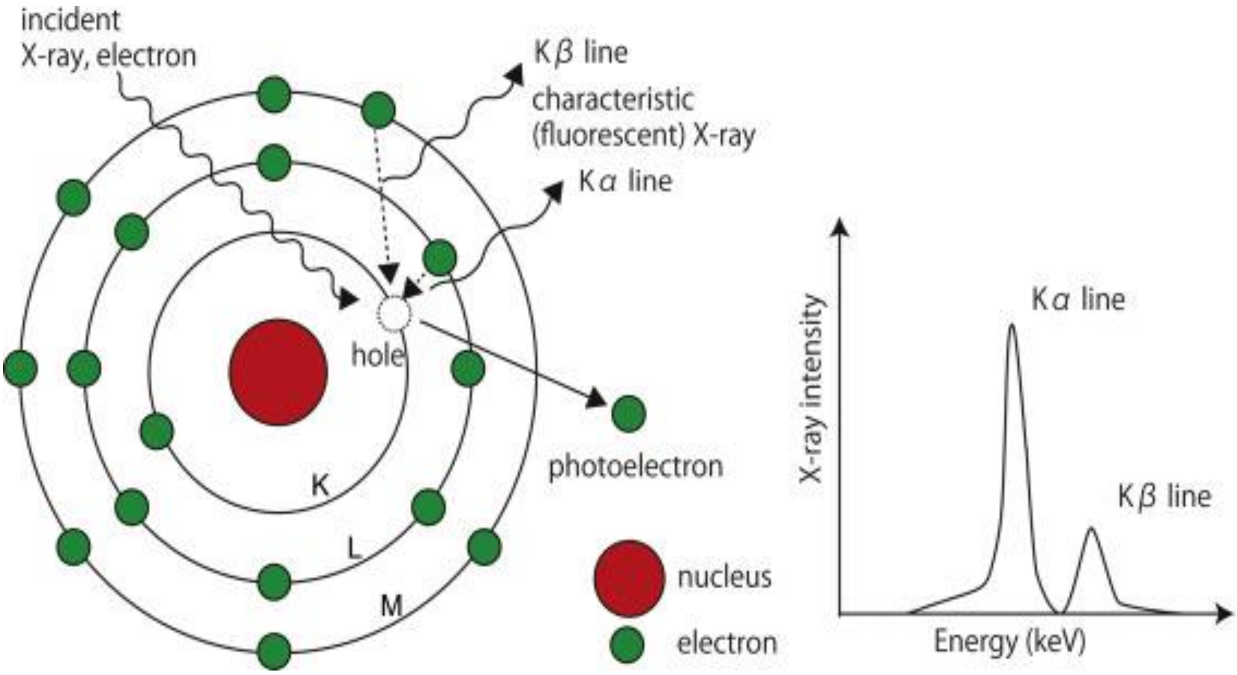

Figure 3.9: Schematic diagram of atomic energy levels with K,L and M-shells [12]

This creates a vacancy in the K-shell. The atom is in the excited state since the electron moves from a higher energy shell (L or M-shell) down to a lower energy shell (K-shell) to fill the empty space in the atom , while some of it energy is released in the form of x-rays which are expressed in electron volts (eV). Kα x-ray is the x-ray photo that is produced when the L-shell electron drops to the K-shell whereas Kβ x-rays are emitted when M-shell electron drops to the K-shell. Kβ x-ray has more energy than Kα x-ray since the energy difference is higher between M and K than L and K [11-12].

3.3.2. Structural characterization technique

3.3.2.1. X-Ray diffraction (XRD)

Description of the technique

XRD is an analytical technique used for characterizing crystalline materials and in the determination of unknown solid, unit cell dimensions, measurements of sample purity and etc.). It is used to obtain structural information about crystalline solids, phase identification of powders before and after annealing [14]. X- ray diffraction is important for solid state physics, materials science, biophysics, medical physics, chemistry and biochemistry. The theory to determine the crystal structure from diffraction was discovered by Bragg in 1915. The Laue's experimental setup for studying single crystal x-ray diffraction is shown below in the **Figure 3.10.**

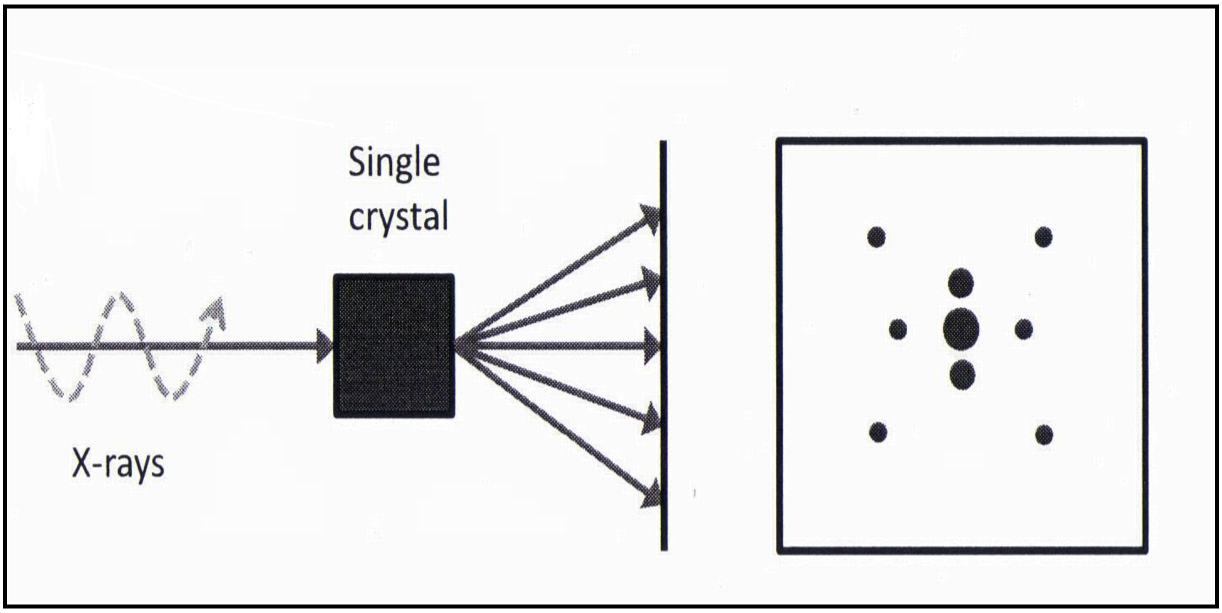

Figure 3.10: Schematic diagram of single crystal showing ordered of spot produced electron beam that passes though single crystal [18].

Nowadays X-rays have been improved by computer technology and have become a popular method for investigating crystalline structures and atomic spacing in solid materials [14]. It is well suited for the characterization of materials with crystalline structure because atoms are arranged in a specific order; the size and shape of the unit cell for any compound can be determined easily using x-ray diffraction. The information obtained from the powder x-ray diffraction is: lattice parameters, phase identity, phase purity, crystallinity, crystal structure and percent phase composition [15].

Operation of the instrument

There are three basic components of XRD, the X-ray tube, a sample holder and the X-ray detector shown in **Figure 3.11** [16].

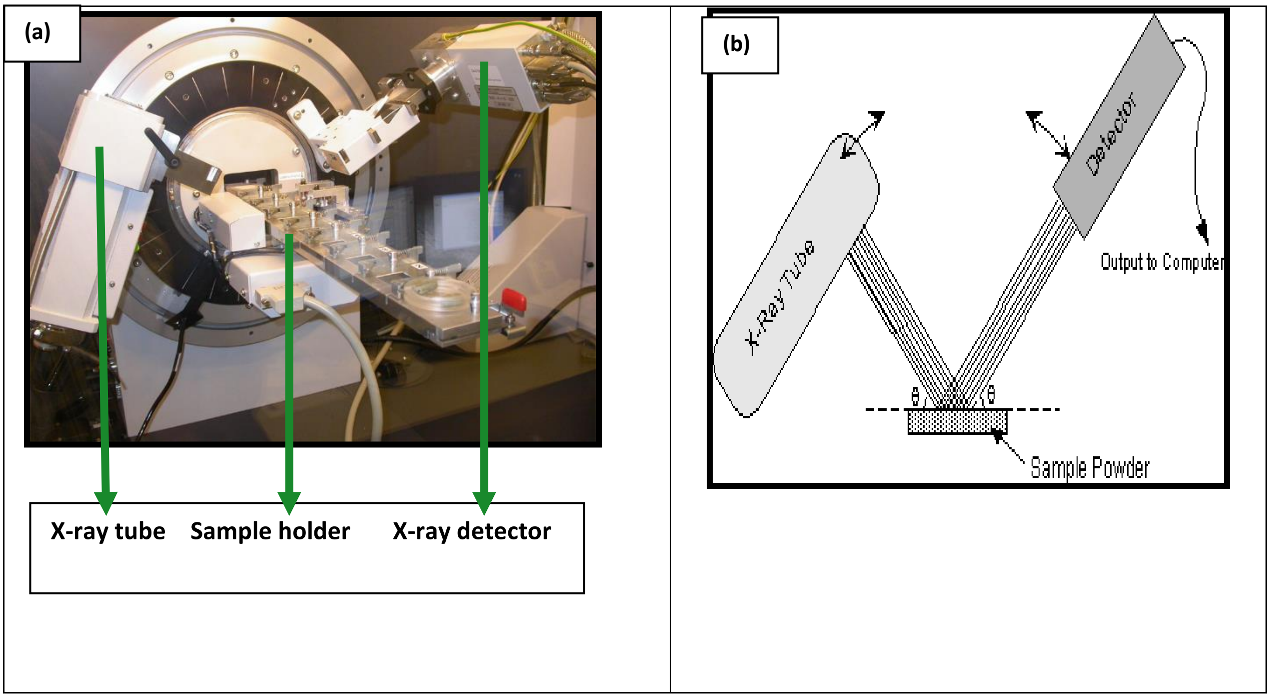

Figure 3.11: (a) Bruker D8 Discover A25 X-ray diffraction instrument and **(b)** schematic diagram showing the setup of XRD technique [16].

The X-ray tube is used to produce X-rays of the same wavelength. A filter is placed in front of an X-ray/cathode ray tube in order to select the X-ray of the same wavelength (monochromatic X-rays) for diffraction. The X-rays are directed parallel towards the position of the sample for the interaction between incident rays and sample to take place. These interactions finally produce constructive interference and diffracted X-rays beam following Bragg's law [16]. A detector will be used to collect the diffracted X-rays and send it to a computer. Diffraction patterns are collected over an extended period of time while the beam intensity remain constant [17]. The diffracted angle is measured between the incident beam and the detector angle which is well explained by the Bragg's law [18].

Bragg diffraction appears equally to neutron diffraction and electron diffraction process [14]. Bragg's law is used to interpret X-ray diffraction data. The diffracted X-rays beams are produced by the interaction between X-rays with the sample, where by these diffracted beams created are related to interplanar spacing in the crystalline powder according to Bragg's law conditions

$$n\lambda = 2d\sin\theta \tag{3.1}$$

Where n is numeric constant known as the order of the diffracted beam, n= 1, 2, 3…, λ- is the wavelength of X-rays, d- is the distance between the lattice planes and θ- is the diffraction angle [17-18].

When an X-ray beam hits the surface of a crystalline sample where the layers of the atoms or ions are separated by an interatomic distance, the diffraction peak is formed when scattered X-rays are produce by a constructive interference. The information of the lattice distance/ spacing and diffraction patterns is obtained by varying the wavelength [14].

(a)

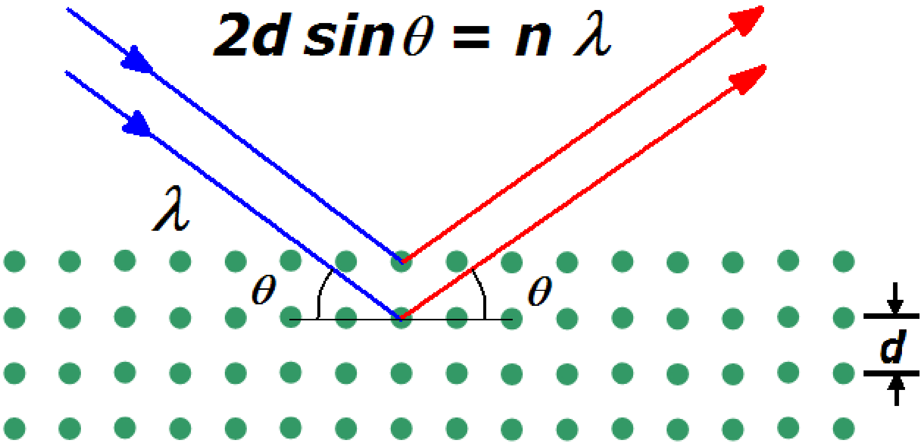

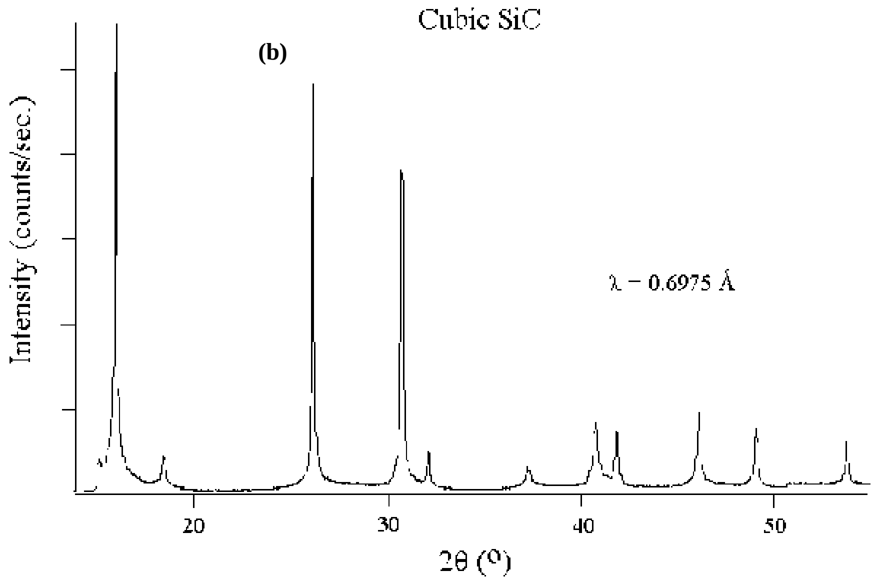

Figure 3.12: (a) Schematic diagram showing the crystals are array of atoms and **(b)** x-ray diffraction pattern of cubic SiC [16].

X-ray diffraction is based on the constructive interference of monochromatic X-rays and crystalline sample. X-rays are generated by the cathode ray tube towards the sample and when the conditions satisfy Bragg's law equation mentioned above, the interaction of incident ray with the sample produces constructive interference resulting in a diffracted ray. This law connects the wavelength of electromagnetic radiation to the diffraction angle and the lattice d-spacing in crystalline sample. The diffracted X-rays are detected, processed and counted through the range of 2θ angle. The intensity plotted against 2θ is illustrated in the **Figure 3.12 (b)**.

Sample preparation

For XRD analysis, the first step was to clean the glass plate with deionized water so that the glass was ready to be used. After the entire cleaning, since the samples were in the dried fine powder form there was no need for grinding. Then, a small amount of powder from each sample was spreaded out uniformly into the glass plate which was amorphous to first get the background of the material. The glass plate was then mounted inside the sample holder in XRD Brucker, D8 advanced with Cu Kα radiation, $\lambda = 1.54060$ Å, with 2θ ranging from 20-90 °C operating at 45 kV and 40 mA.

3.3.3. Optical characterization technique

3.3.3.1. Fourier Transform Infrared Spectroscopy (ATR-FTIR)

Description of the technique

Fourier Transform Infrared Spectroscopy (FT-IR) is an important technique in organic chemistry, it is used to identify the specific functional groups that are present in a material, where by the absorption bands can be used to confirm the pure compound or detect the presence of specific impurities and it has been widely used in the structure analysis produced using chemically or natural methodology. FT-IR is used for quantitative analysis in almost all fields of science for over seventy years and it has various advantages and applications more than dispersive infrared technology [19]. It was developed in order to overcome the limitation experienced with the dispersive instruments which has a slow scanning process [20].

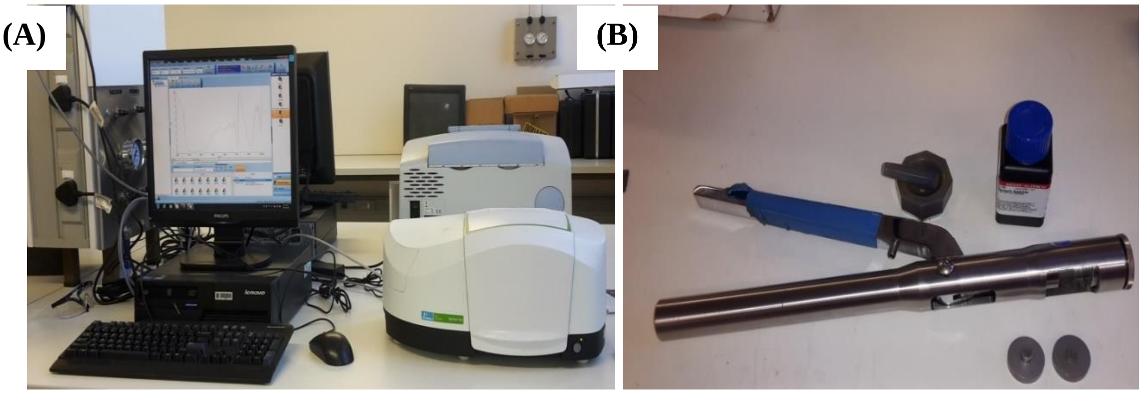

Figure 3.13: (a) FT-IR spectrometer (PerkinElmer, 95058) that has been used during the project (**b)** the KBr, mortar and a pastle as a well as hydraulic press.

In FT-IR all frequencies are measured at the same time in an interferometer with Fourier transmission and measurement time reduced in a multi-wavelength measurement and it also allows chemical reaction to be monitored. FT-IR is 100 times better than a dispersive, it can quantify the entire wavelength range and it has a very stable frequency which makes it to have an essential long term stability, repeatability in the spectrum and it can also measure the samples with high carbon content [21].

Most of Fourier transform spectrometers nowadays still make use of Michelson interferometer. Once the spectrum is collected the work begins. The spectrum has two general areas, the functional groups (4000 -1500 cm^{-1}) and the finger print region (1500-400 cm^{-1}). The peaks in functional group region are properties of the particular kinds of bonds and can be used to investigate where a certain functional group is present. The peaks in fingerprint region comes from the complex deformation of molecules, they contain various types of bonds which comes from the multiple bonds deforming simultaneously. FT-IR identify unknown materials, discover the quality of the sample and also identify the amount of component within the sample [20, 22-23].

FT-IR spectroscopy includes absorption, reflection, emission spectrum obtained by Fourier transform of an optical interferogram [24]. They have the speed, accuracy and sensitivity compared to dispersive spectrometers and allow a lot of analysis of micro samples to nanogram making the FT-IR an extremely useful tool for problem solving in many studies. In the FT-IR spectroscopy, a sample is displayed to an electromagnetic radiation. The energy of the incident radiation is varied over the potential range and the results are plotted as a function of frequency of incident radiation. To identify the sample a series of peaks in the spectrum will be used which are produced from the radiation absorbed [24].

Operation of the instrument

The FT-IR spectrometer diagram shown below in **Figure 3.14**, consists of an IR source, a Collimator, a beam splitter, fixed & moving mirrors, a sample cell and a detector, connected to interferometer. All of them use the same beam splitter and mirror.

The IR goes through the sample where by the certain IR are absorbed by the sample and some are transmitted. The spectrum obtained exhibit the molecular transmission and absorption producing the sample molecular fingerprint. However, a fingerprint no two different compounds molecular structure generates the same infrared spectrum. Several types of analysis can be done by infrared spectroscopy. The computer controls the optical components, collects and stores information, perform calculations on the data and displays spectra.

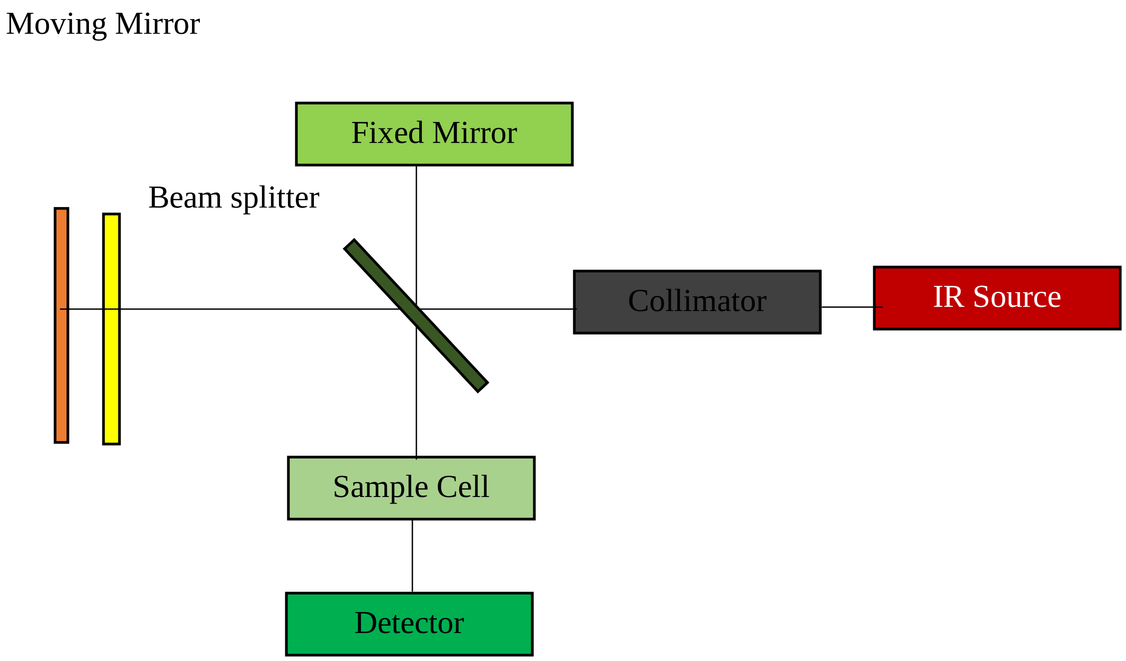

Figure 3.14: The diagram of FT-IR spectrometer [19].

Sample preparation

In the FT-IR investigation, the samples were mixed with the KBr from Fluka, Germany since it has large transmission window. Small amount of Eu_2O_3 nanopowder were mixed with the KBr, in order to obtain an accurate spectra the mixture was blended using a mortar and a pastel. The obtained powder was then compressed into pallets using the hydraulic press (Beckman 00-25 Glenrothes five scottland) for the pallets to be ready for FT-IR analysis.

3.3.3.2. Raman Spectroscopy

Description of the technique

Raman spectroscopy is a powerful technique for structural characterization and chemical composition of materials (physical form of molecules identification of substances from the characterization spectral patterns and quantitative determination of the amount of substances in a sample). It is a non-destructive optical molecular spectroscopic imaging technique, non-invasive and interesting choice for analytical tasks [25].

It has become an important tool in research, mostly used in chemistry for chemical bonds and symmetry of molecules. It’s also used in medicine for respiratory gas mixtures during surgery as well as in bio-pharmaceuticular industries to investigate the pharmaceuticular ingredients. In this project, Raman spectroscopy has been used as complementary technique to FT-IR to analyse the Eu_2O_3 nanoparticles.

Operation of the instrument

This is a scattering technique where by the frequency of monochromatic is different from the frequency of small fraction of scattered radiation. The monochromatic laser beam illuminates the sample to interact with molecules of a sample to produce a scattered light which has a frequency different from the incident light and exhibits a spectrum. The inelastic collision between incident monochromatic radiation and molecules of sample are used to produce the Raman spectra. When the frequency of the incident radiation is equal to the monochromatic radiation that strikes the sample, it forms Raleigh scattering. Raman scattering is formed when a frequency of scattered radiation is different from the frequency of incident radiation. The stokes line that tend to show up on the Raman spectrum when the frequency of scattered radiation is lower than frequency of incident radiation. In this case, the incident radiation transfers the energy to the samples and it scattered with the red shifted frequency. But when the scattered radiation is higher than the incident radiation the anti-stokes line showing the blue shifted frequency are formed in the spectrum of Raman as shown in **Figure 3.15 below**. Raman spectrum is presented as intensity versus wavelength shift [26].

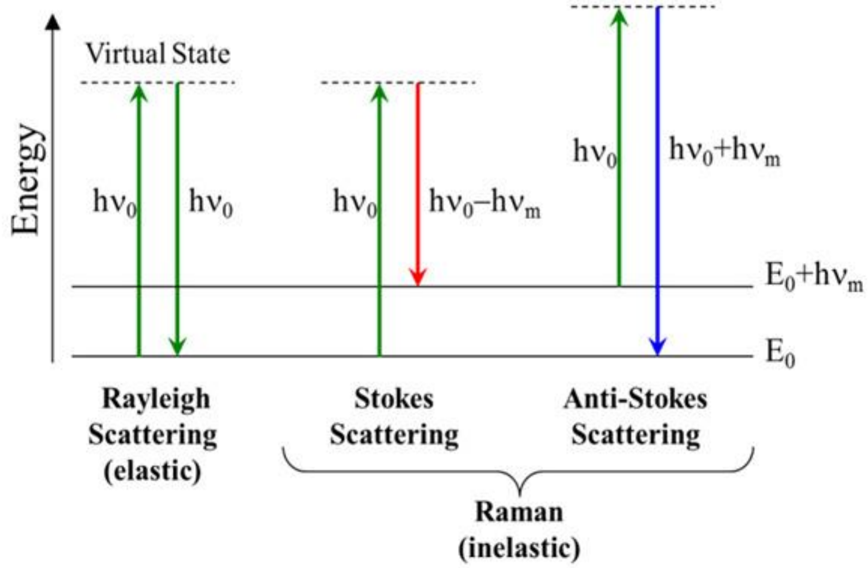

Figure 3.15: Diagram representing the quantum energy transitions of Rayleigh and Raman scattering [27].

3.3.3.3. Ultraviolet and visible (UV-Vis-NIR)

Description of the technique

Ultraviolet and visible (UV-Vis) spectrometer have been well established for last 35 years and have become the most important analytical instrument in the modern laboratories. It was originally developed for absorption measurements of liquid samples, in nowadays high energy spectrometer is increasing due to the rapid increasing reflection and absorption measurement on materials including semiconductors, films, glasses and other absorbing materials [29]. UV-Visible spectrometry has been used due to its simplicity, versatility, speed, accuracy and cost-effectiveness. Nanoparticles have the optical properties that are delicate to size, shape, concentration and agglomeration state which makes UV-Vis-NIR spectroscopy an essential tool for investigating, characterizing and studying these materials [31]. Nanoparticles strongly interact with the specific wavelengths of light and the authentic optical properties of each material. UV-Vis is widely used in the analytical chemistry for the quantitative determination of different analytes such as transition metal ions, highly conjunged organic compounds and biological macromolecules and is well established in solution but solid and gases may also be studied.

This instrument measures the reflection or the absorbance characteristics of a material and it is design to make wavelength of radiation that will to be narrow. The electromagnet radiation wavelengths are defined as follows [30]: UV-300 to 400 nm, VIS-400 to 765 nm and NIR-765 to 3200 nm

Operation of the instrument

Radiation is a stream of particles known as photons. Atoms and molecules exist in a number of defined energy levels and change of levels requires the absorption or emission of an integral number of a unit of energy called photon.

The energy of a photon is absorbed or emitted during the transition from one molecular energy level to another as illustrated by the equation below:

$$E = hv \tag{3.20}$$

Where h is the Plank's constant and v is the frequency of the photon.

To the band energy gap/ energy

$$E = hc/\lambda \tag{3.21}$$

where $c = v\lambda$, c is the speed of light.

The shorter the wavelength, the greater the energy of the photon and similarly, the longer the wavelength the lower the energy of the photon becomes. A molecule of any substance has an internal energy, which can be considered as the total sum of electron energy of vibration between atoms and radiation of molecules energy. Electronic energy state of simple molecules are common separated, most only the absorption of high energy photon with short wavelength because they excite molecule from ground to excited state, see the figure that follows:

Materials absorb light in areas near ultraviolet and visible regions. Photon near ultraviolet and visible light can affect the transition. The electronic state of molecules changes as the sample absorbs the light in the ultraviolet or visible region.

The absorption energy supplied by the light promotes electrons from ground state level to higher energy, excited state or anti-bonding orbitals where by three potential types of ground state orbitals may be involved : σ strong molecular bonding, π weak molecular bonding, n non-bonding atomic orbital. In addition, two types of anti-bonding orbitals may be also involved in the transition σ^* sigma star orbital and π^* pi star orbital. These electron transitions can occur by the absorption of ultraviolet and visible light see **Figure 3.15** below illustrating the general pattern of the energy levels and the fact that the transitions are brought by the absorption of different amount of energy.

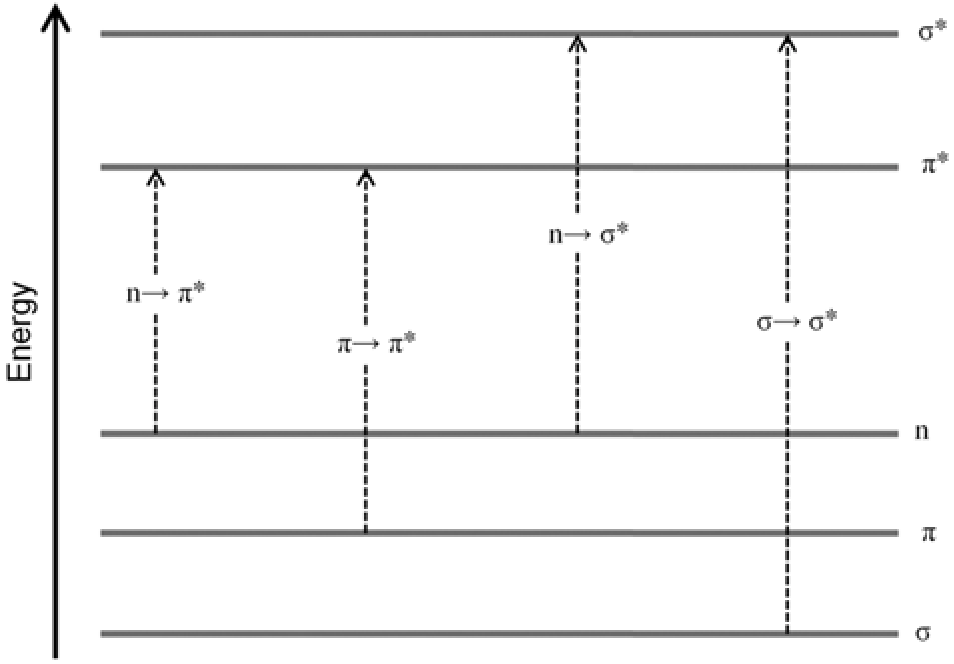

Figure 3.16: Schematic diagram showing the general pattern of the energy levels [31].

Both to σ to σ* and n to σ* transition require a great energy and occur in the far ultraviolet region below 200 nm. Consequently saturated group do not slow the strong absorption in the ordinary ultraviolet region. The transition of n to π* and π to π* absorption occur in the molecules with unsaturated centers near ultraviolet, they require less energy and occur at longer wavelength than transitions to σ* [30-31].

Sample preparation

The Eu_2O_3 nanopowders were first dissolve into ethanol in the ultrasonic bath for approximately 10 minutes. The dissolved samples were collected with the quartz cuvette (~2.00 mm) to the sample holder between the light source and a photodetector to transmit the radiationin the UV-Vis spectroscopy. The optical properties of the samples were then measured with a UV-Vis NIR spectrometer. The spectrometer has the most general sources deuterium lamp for UV- region and halogen for the visible region to cover the entire wavelength range. It’s combined with the fluorescence analysis/ measurements absorption band broadening and consequent reduction structural resolution and ε_{max} [30].

3.3.3.4. Photoluminescence (PL)

Description of the technique

Photoluminescence spectroscopy is non-destructive contactless and very common spectroscopy used to study the electronic structure and the optical properties of nanomaterials [32]. There are different forms of photoluminescence namely phosphorescence, fluorescence and resonant radiation.

Operation of the technique

It consists of the light source, excitation monochromator, sample cell and emission monochromator with a detector in the **Figure 3.17** below.

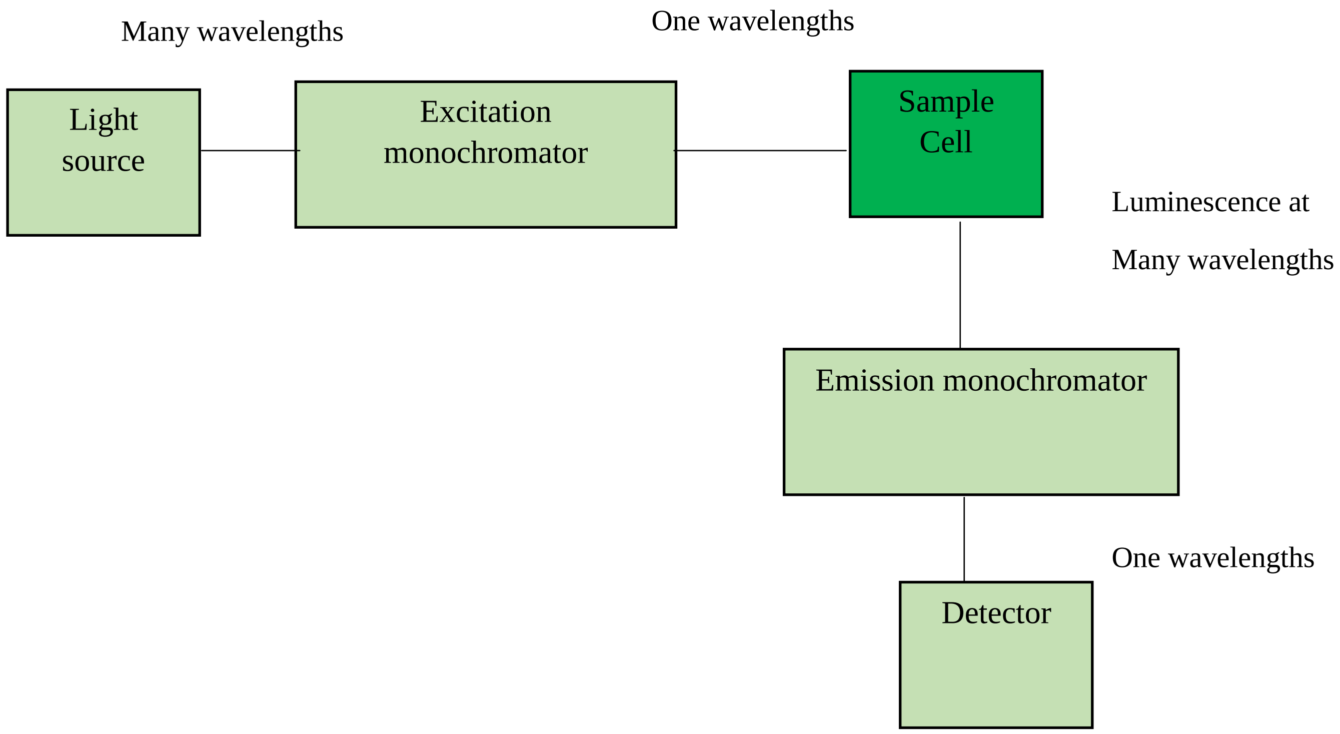

Figure 3.17: Schematic representation of Luminescence setup.

For PL measurements, the same procedure used for the sample of UV-Vis was followed. An emission is discovered over a series of wavelength after the sample is illuminated at a single wavelength and the emission monochromator picks up one wavelength and excitation monochromator also picks up one wavelength at a time to detect [32].

The light is absorbed when it strikes the samples and transmits the excess energy into the material via the photo- excitation process. One way this excess energy can be abandoned by the samples is via the emission of light. The material has electrons, these electrons move into permissible excited state caused by force from the photo-excitation. The excess energy will be then delivered and may involve the radioactive or non-radioactive process when these electron within the material return to their equilibrium states.

The photoluminescence is involved in the distinction of energy levels in across electron states included in the transition between the equilibrium state and excited state. The amount of the emitted light is involved to the considerable contribution of the emission of light [33]. Photoluminescence spectroscopy is a good methodology for luminescence characterization investigation.

3.4. References

1. B. Voutou, E. Stefanaki, ‘Electronic Microscopy: The basics, Physics of advanced materials winter school’, (2008).
2. Cryo-electron microscopy, ‘Introduction to Electron Microscopy’, (2015).
3. A. Dubey, ‘Scanning Electron Microscope and transition’, Technology, (2013).
4. J.S. Arino, ‘Scanning Electron Microscopy’, Central bicol state university of education, Power point presentation.
5. W. Lin, ‘Microscopic Composition Measurement at nanoscale’, The data storage systems center (DSSC) power point presentation, April (2005).
6. D.B. Williams, C.B Carter, ‘Transmission Electron Microscopy’, A textbook for materials science, Second edition, Chapter 2, page 3-4
7. S. Bhargava, ‘Scanning Electron Microscopy (SEM)’, Lecture (2016).
8. G.S. Salunkhe, ‘Scanning Electron Microscope’, 2nd MDS Oral and maxillofacial pathology (2014).
9. K. Akhtar, Mechanical-4C(1).
10. ‘Radiological and environmental management’, Purdue university, pdf (2014).
11. J. Wiley & Sons, ‘Energy dispersive spectroscopy’, Second edition, (2015).
12. M. Uo, T. Wada, T. Sugiyama, ‘Application of X-ray Fluorescence Analysis (XRF) to dental and medical specimens’, Japanese dental science review, Vol.51, 2-9 (2015).
13. ‘Transmission Electron Microscopy’, September (2004).
14. E. Day, S. Ross, ‘X-ray Diffraction’, Advanced lab 1, Power point presentation, (2004).
15. H. Zurloye, ‘X-ray Diffraction’, University of South Carolina, pdf.
16. B.L. Dutrow, C.M. Clark, ‘X-ray Powder Diffraction (XRD)’, Geochemical Instrumentation and Analysis, Louisiana State University.
17. W. Lin, A.R. Barron, ‘An introduction to X-ray Diffraction’, Connexion Module , (2011).
18. J.R. Connolly, ‘Introduction to X-ray Powder Diffraction’, 1-9 (2007).
19. S.D. Sawant, A.A. Baravkar, R.N. Kale, ‘FT-IR Spectroscopy: Principle,techniques and mathematics’, Journal of pharma & bioscience, vol. 2, (2011).
20. ThermoNicolet Corporation, ‘Introduction to Fourier Transform Infrared Spectroscopy’, pdf, (2001).

21. P. Elmer, ‘Principles of FT-IR, Human health environmental’, Power point presentation, (2009).

22. ‘FT-IR Spectroscopy’, Department of Chemistry, Oregon State University, (2015).

23. R.A. Musash, ‘Mass Spectrometry and Infrared Spectroscopy’, Organic Chemistry, Chapter 13, Second edition, State University of New York.

24. D.R. Vij editor, ‘Handbook of the applied solid state spectroscopy’, Kurukshetra University, India (2006).

25. Q. Wang, ‘Raman Spectroscopic Characterization and Analysis of Agricultural and Biological System’, (2013).

26. G.S. Bumbra, R.M. Sharma, ‘Raman Spectroscopy: Basic principle, instrumentation and selected application for the characterizations of drug abuse’, Journal of forensic science, vol. 6, 209-215 (2016).

27. ‘Theory of Raman’, Scattering BWTEK.

28. D.W. Hahn, ‘Raman Scattering Theory’, Department of mechanical and aerospace engineering, University of Florida, (2007).

29. Shimadzu Europa GMBH analytical and measuring instrument, pdf.

30. ThermoSpectronic, ‘Basic UV-Vis Theory’, Concepts and Application, pdf.

31. ‘UV/VIS/IR Spectroscopy analysis of nanoparticles’, vol 1.1, (2012).

32. R. Ye, A.R. Barron, ‘Photoluminescence Spectroscopy & it applications’, Version 1.2, (2011).

33. D. Herman, ‘Photoluminescence Spectroscopy’, North University, (2004).

CHAPTER FOUR: RESULTS AND DISCUSSIONS

4.1. Surface Morphology characterization

The SEM and HRTEM experiments were performed to determine the surface morphology of Eu_2O_3 samples annealed at 300°C, 500°C and 700°C. SEM analysis was performed using Carl Zeiss Auriga Field Emission Scanning electron microscope (FEG SEM) imaging at 5 keV and Fei tecnai $G^2$2O, HRTEM with Field Gun Resolution TEM operating at a 200 kV.
The EDS pattern for elemental analysis corresponding to both SEM and HRTEM micrograph existing on the Eu_2O_3 NPs were obtained using an oxford instrument X-max solid state silicon drift detector at 20 keV.

4.1.1. Scanning Electron Microscopy (SEM)

The as-prepared particles were dried in a standard oven set at ~100°C and were annealed at different temperatures (300, 500 and 700°C) to obtain the pure Eu_2O_3 NPs. After annealing, the colour of powders changed from greyish brown to black at 300°C and white at 500°C and 700°C. The Eu_2O_3 powders were coated with gold and palladium for conductivity and charge effects minimization on the carbon coated grid using a coating sputter coater and SEM analysis was performed.

Figures 4.1, show the SEM images of small Eu_2O_3 NPs formed. It can be established that the Eu_2O_3 NPs are nano-scaled with a mixed population of crystalline particles. SEM images show that the particle size become slightly bigger and more homogeneous after calcination, which is in agreement with previous results [1]. The powder consists of different shapes edge nano-scaled particles which reflect a high degree of crystallographic symmetry like a cubic phase. **Fig. 4.1 (1)**, reports on a characteristic SEM micrograph obtained after annealing at 300°C, very small NPs were formed and (b) at 100 K X of magnification was more better than (a) 20.0 K X magnification. **Fig. 4.1 (2)**, reports SEM images annealed at 500°C, which reveals small sphere-like particles and as you increase the temperature the size of the NPs also increase. **Fig. 4.1 (3)**, shows a typical SEM images of Eu_2O_3 NPs annealed at 700°C. It consists of different shapes of particle size cubic phase.

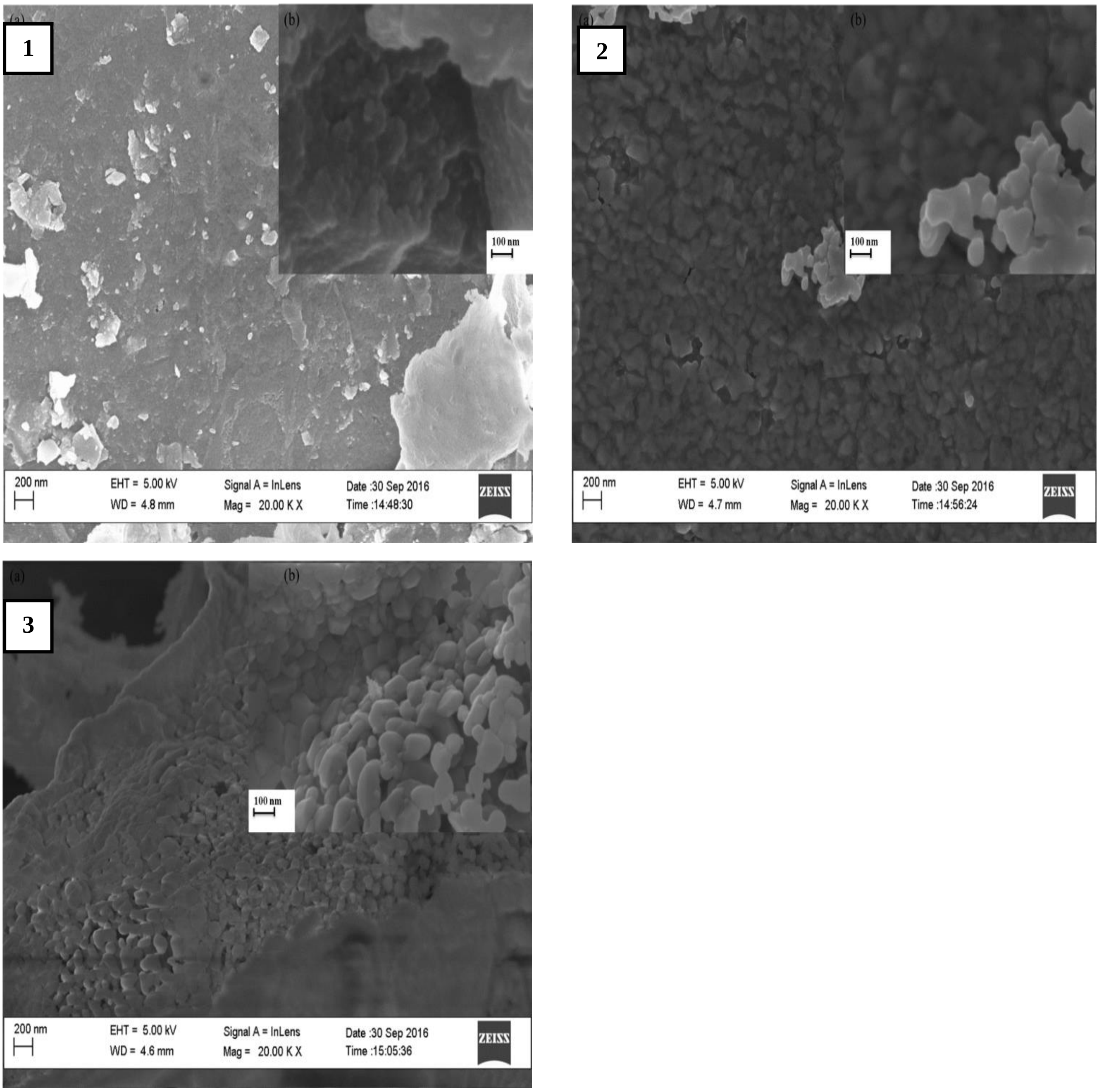

Figure 4.1: SEM images of the Eu_2O_3 NPs annealed at **(1)** 300, **(2)** 500 and **(3)** 700 ^{o}C in air for 2 h showing different scale bar, **(a)** 200 nm and **(b)** 100 nm.

4.1.2. High Resolution Transmission Electron Microscopy (HRTEM)

To confirm the obtained SEM results, the microstructure and surface morphology analyses of annealed Eu_2O_3 powder at 300, 500 and 700^oC were performed using High resolution transmission microscopy (HRTEM). HRTEM was also used for Electron Diffraction (SAED) to investigate the crystallinity of nanoparticles analysis.

For the HRTEM measurements, the annealed Eu_2O_3 powder was first dispersed in to ethanol in the ultrasonic bath and was then coated with copper grids. **Figures 4.2** exhibits the typical HRTEM images of Eu_2O_3 nanoparticles annealed at 300, 500 and 700^oC.The powder as observed from the images, consists of agglomerated shape-edge nanoscale particles having different shapes which possess a high degree of crystallographic symmetry confirming cubic phase. As observed from the images of HRTEM, all the produced nanoparticles possess different shapes.

They consist of agglomerated shape edge nano-scale particles. The selected area electron diffraction (SAED) analyses were performed in order to investigate the crystallinity of the nanoparticles, from such observations the Eu_2O_3 nanoparticles are polycrystalline (composed of many crystals) with the body centered cubic crystal structure. This oxide has a number of structural phases known as A-type hexagonal, B-type monoclinic and C-type cubic phase. These are in order of $C \rightarrow B \rightarrow A$ when the temperature is increased new phases are formed, as one can distinguish between 300 – 700^oC that at lower temperatures better results are obtained. The inter-reticular distances were also measured as shown in **Figures 4.2 (1-3)** respectively. The distance of the lattice fringes observed were found to be 0.3 & 0.22 nm for 300^oC, 0.36 & 0.28 nm for 500^oC and 0. 27 nm for 700^oC which are in good agreement with Eu2O3 [222] $d_{(222)}$= 0.313 nm and [400] $d_{(400)}$= 0.271 nm reticular planes. The discovered inter-reticular distances between the lattice fringes are consistent with the previous results reported by kattel et al. and Diallo et al [5-6]. and are also in agreement with Eu_2O_3 cubic phase.

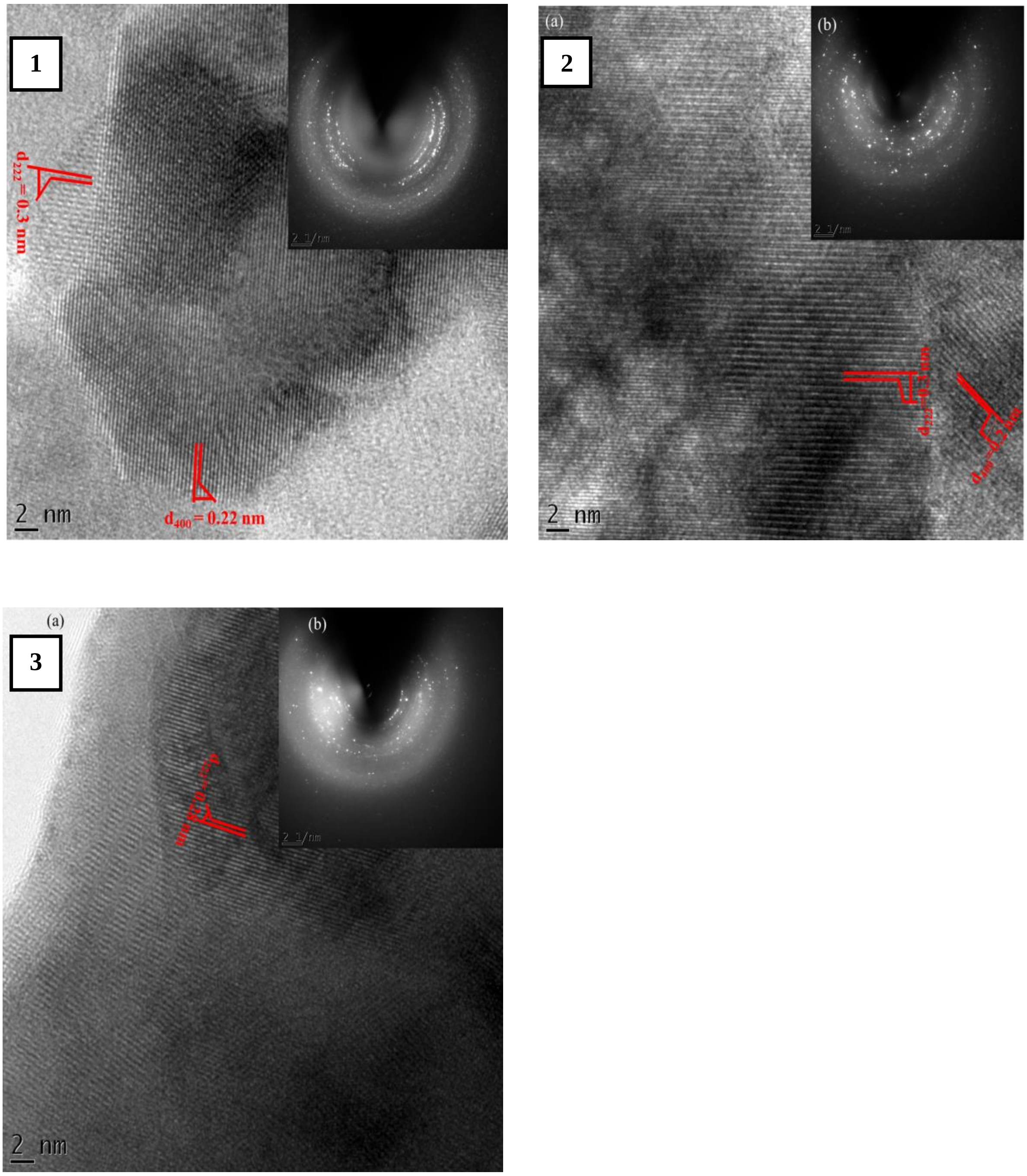

Figure 4.2: (a) HRTEM of the Eu_2O_3 NPs annealed at **(1)** 300, **(2)** 500 and **(3)** 700 °C in air for 2 hrs, and **(b)** their typical selected electron diffraction pattern.

4.1.3. Energy dispersive x-ray spectroscopy (EDS)

To further determine the purity of Eu_2O_3 samples, Energy Dispersive X-ray Spectroscopy (EDS) microanalysis was conducted to reveal the elements that exist within the Eu_2O_3 NPs using an EDS Oxford instrument X-max Solid State silicon drift detectors at 20 keV. Several peaks of Eu indicated in (**fig. 4.3 - 4.5**) were observed together with peaks of other elements namely O, C, Ca, Mn, P, Cl, S and K signals. The Eu peaks are related to the Eu_2O_3 nanoparticles, O can only be due to Eu_2O_3 nanoparticles and the C originates from the carbon coated grid during experiment preparation for the conductivity and charge effects minimization [6].

The presence of other elements such as C, Ca, Mn, P, Cl, S and K originates from natural extract of *hibiscus sabdariffa* flowers as observed in other biosynthesized nano metal oxides. EDS also revealed that at high temperatures, the most abundant element are Eu and O, 66.58 wt% and 20.14 wt%, as shown in **Table 4.1 below**. It was found that after annealing at 500 and 700 ^{o}C, some based compounds from the natural extract begin to decompose.

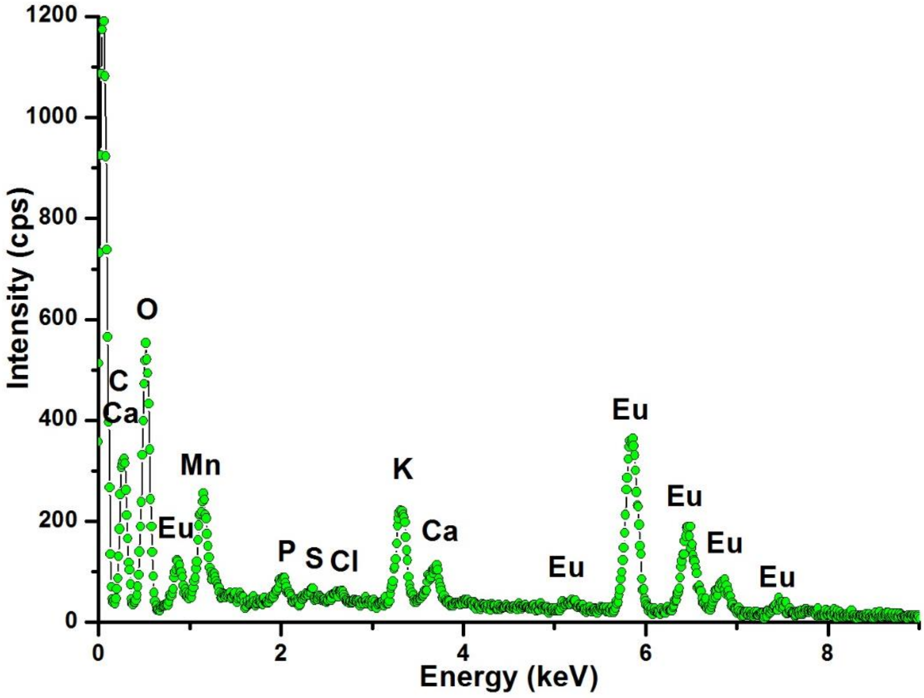

Figure 4.3: Typical EDS spectrum of the Eu_2O_3 NPs, annealed at 300^{o}C measured from the SEM micrograph (**Figure 4.1 (1)**)

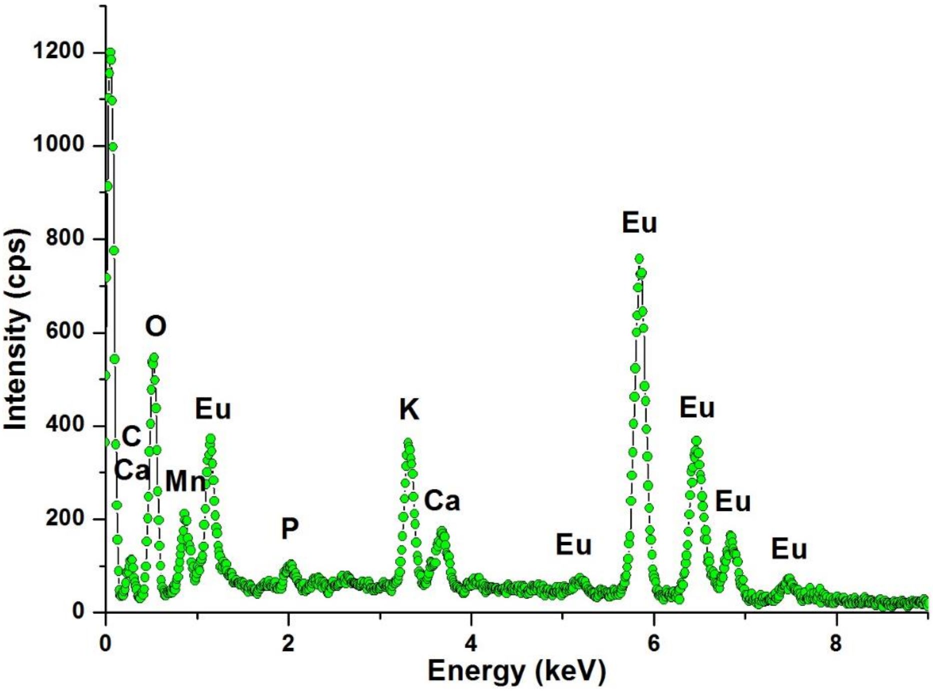

Figure 4.4: Typical EDS spectrum of the Eu_2O_3 NPs, annealed at 300^{o}C measured from the SEM micrograph (**Figure 4.1 (2)**).

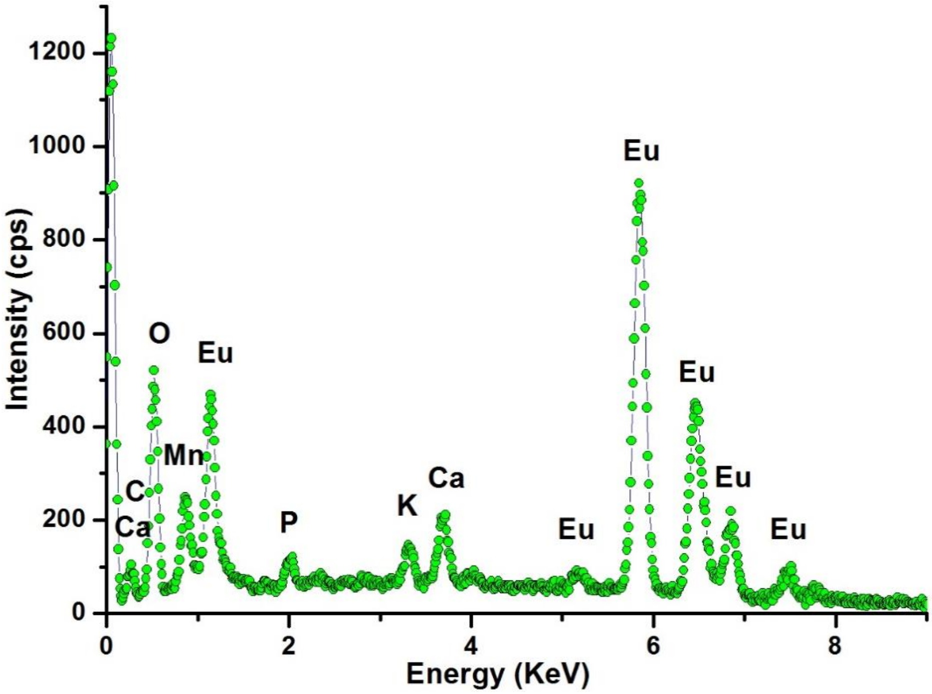

Figure 4.5: Typical EDS spectrum of the Eu_2O_3 NPs, annealed at 700^{o}C measured from the SEM micrograph (**Figure 4.1 (3)**).

Table 4.1: The EDS data showing spectra data of the chemical composition of Eu_2O_3 NPs annealed at 300, 500 and 700 °C.

300°C	**wt%**	**wt% sigma**	**500°C**	**wt%**	**wt% sigma**	**700°C**	**wt%**	**wt% sigma**
C	34.46	3.73	C	10.55	4.75	C	5.78	5.19
O	29.5	1.79	O	24.55	1.43	O	20.14	1.24
P	0.4	0.23	P	0.68	0.31	P	0.75	0.35
S	0.24	0.08	K	4.91	0.31	K	1.26	0.14
Cl	0.27	0.08	Ca	1.76	0.16	Ca	2.32	0.18
K	2.93	0.21	Mn	2.74	0.46	Mn	3.18	0.49
Ca	1.12	0.12	Eu	54.8	2.98	Eu	66.58	3.73
Mn	1.4	0.34						
Eu	29.69	1.78						
Total:	100		**Total:**	100		**Total:**	100	

4.2. Structure characterization

4.2.1. X-ray Diffraction (XRD) analysis

X-ray diffraction was performed for phase identification of Eu_2O_3 nanoparticles at room temperature , using Bruker Advanced D8 diffractometer with monochromated Cu Kα radiation of wavelength λ = 1.54060 Å operating at a current of 40 mA and a voltage of 40 kV in the Bragg-Brentano geometry. **Figure 4.6, 4.7** and **4.8** shows XRD profile of the annealed Eu_2O_3 NPs.

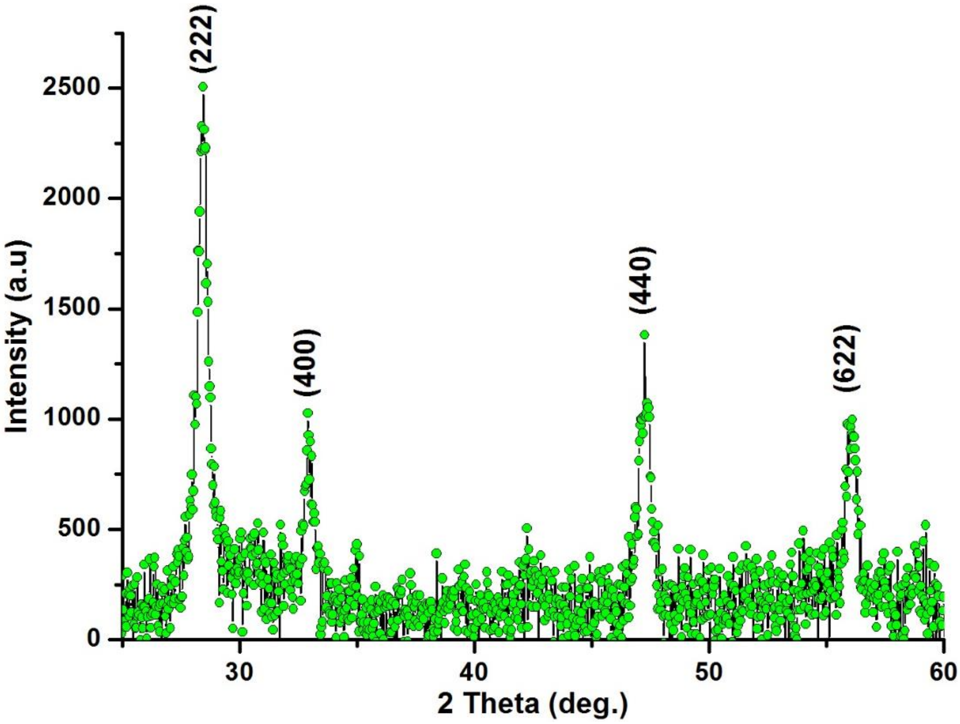

Figure 4.6: X-ray diffraction pattern obtained from Eu_2O_3 NPs annealed at 300°C.

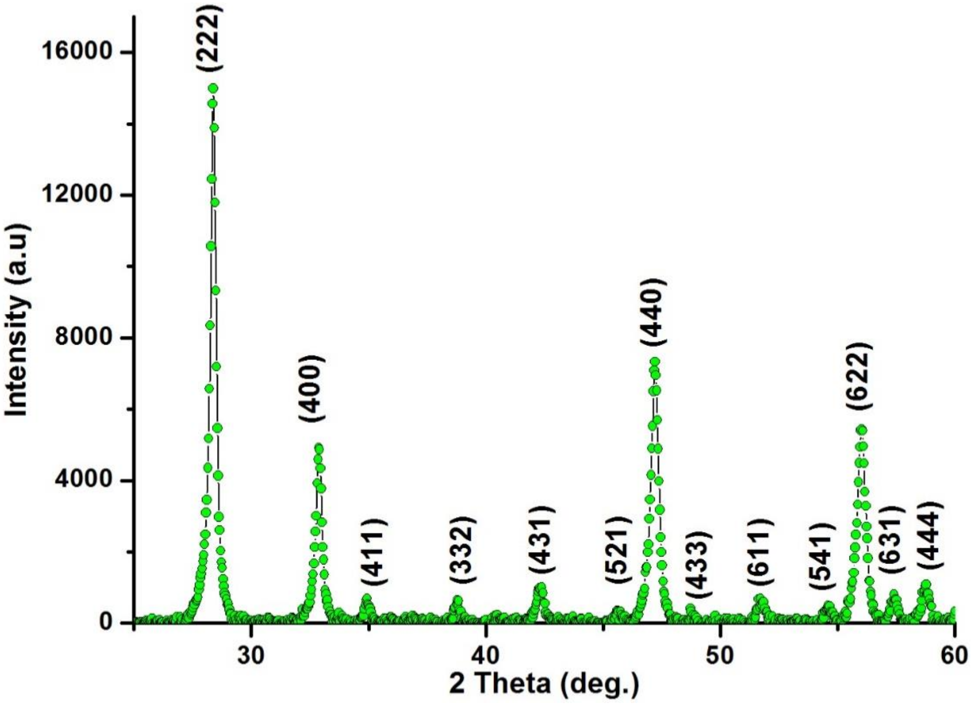

Figure 4.7: X-ray diffraction pattern obtained from Eu_2O_3 NPs annealed at 500^oC.

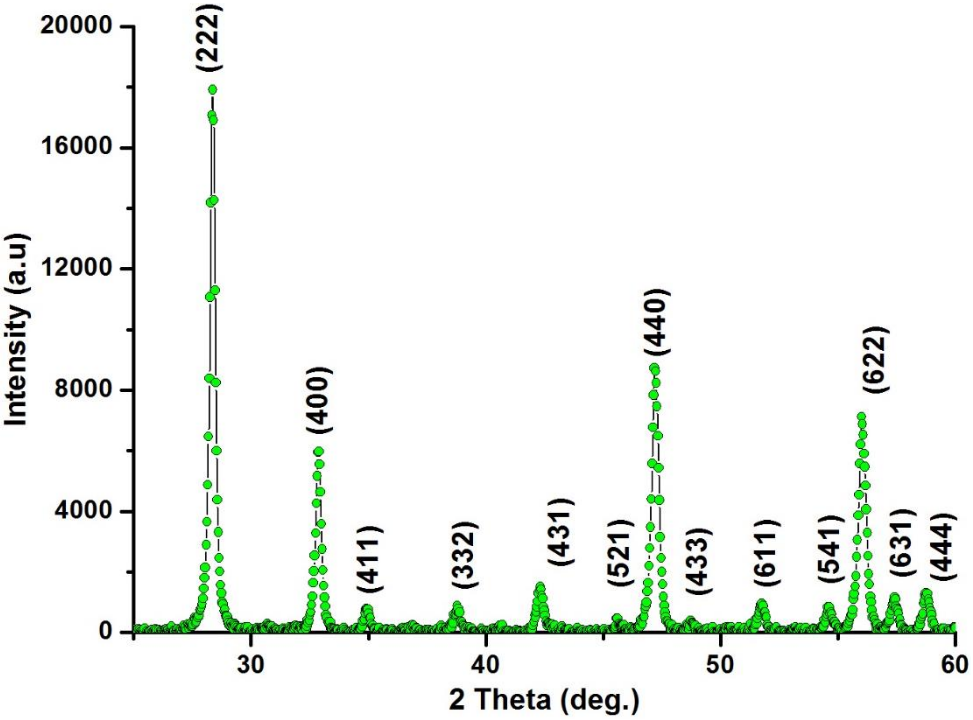

Figure 4.8: X-ray diffraction pattern obtained from Eu_2O_3 NPs annealed at 700^oC.

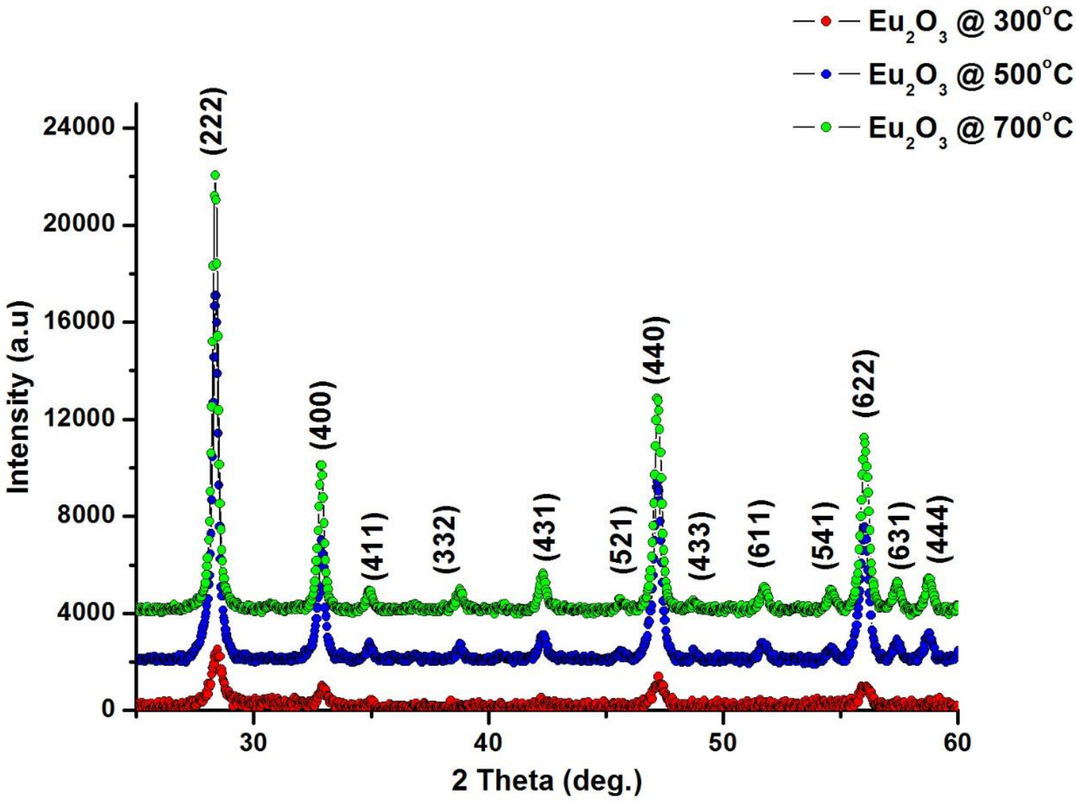

Figure 4.9: The overlay X-ray diffraction patterns obtained from Eu_2O_3 NPs annealed for 2hrs at 300, 500 and 700°C.

Figure 4.9 shows the XRD profile obtained after annealing at different temperatures, 300°C, 500°C and 700°C in the 2θ angular range of 20 to 60 degrees. Before annealing, no peaks were observed, showing that the material was amorphous and after annealing at 300°C, 500°C and 700°C for 2hrs each, the nanopowder changed from yellow to black at 300°C and white at 500°C and 700°C the XRD patterns were drastically observed and corresponding very well to JCPDS 00-034-0392 that Eu_2O_3 belongs and Bravais lattice with the space group Ia-3 and unit cell lattice bulk parameters $a_{bulk}= b_{bulk}= c_{bulk} = 10.86830$ Å of body centred cubic phase of Eu_2O_3 [2, 4-5]. The presence of several broad Bragg peaks was centred at 28.422, 32.927, 34.990, 38.839, 42.363, 47.267, 51.809, 54.682, 56.078, 57.453 and 58.813 degrees correspond to (222), (400), (411), (332), (431), (440), (433), (611), (541), (622), (631) and (444) planes. These peaks indicates that there is no impurity phase among the material. It can also be seen that the diffraction peaks of the samples are very sharp and strong revealing that material is high in crystallinity, the four major peaks was found at 28.422, 32.927, 47.267 and 56.078 which corresponds to the (222), (400), (440) and (622) planes. The grain size of nanoparticles was calculated for each sample using Debye-Scherrer approximation $D= 0.9 \lambda/ \beta\cos\theta$, where λ is the wavelength, β is the quartz standard corrected full width at half maximum (FWHM) of the Bragg peak, the values were extracted from the XRD pattern simulation and θ is the Bragg angle. The average size of NPs ranges within 14 nm to 25 nm, corresponds well to the literature because the size of the cubic-like particles found within 10-26 nm range **(Table 4.2 - 4.4)**. The calculated lattice constant using the relation $\frac{1}{{d_{hkl}}^2} = \frac{h^2+k^2+l^2}{{a_{exp}}^2}$ was $a_{exp} = 10.87812$ Å slightly larger than the bulk value $a = 10.86830$ Å on JCPDS 00-034-0392.

It was observed that the nanoparticles increase in size as the temperature increases. As the temperature is increased, the peaks become sharper and narrow which confirms the stabilization of NPs capping agent and also the crystalline nature of Eu_2O_3.

Additionally, the narrow and strong peaks indicate that Eu_2O_3 NPs have a good crystallinity pattern [3, 6]. The results are in good agreement with the ones reported by Yue Li et al. and Diallo et al.

Table 4.2: Main characteristics of the XRD Bragg peaks of the Eu_2O_3 powder annealed at 300°C in air for 2h.

Plane(hkl)	**$2\theta_{(exp)}$ (deg)**	**$\theta_{(exp)}$ (deg)**	**$\theta_{(exp)}$(rad)**	**d_{exp} (Å)**	**FWHM(rad)**	**Average edge size (nm)**	**a_{exp}(Å)**
222	28.44	14.222	0.24	3.14	0.00955114	149.76	10.86
400	32.95	16.47	0.28	2.72	0.010003878	144.54	10.86
440	47.26	23.63	0.41	1.92	0.011094185	136.42	10.87
622	56.05	28.02	0.48	1.64	0.009950297	157.86	10.87
						147.14	10.86
						14.71	

Table 4.3: Main characteristics of the XRD Bragg peaks of the Eu_2O_3 powder annealed at 500°C in air for 2h.

Plane(hkl)	**$2\theta_{(exp)}$ (deg)**	**$\theta_{(exp)}$ (deg)**	**$\theta_{(exp)}$(rad)**	**d_{exp} (Å)**	**FWHM(rad)**	**Average edge size (nm)**	**a_{exp}(Å)**
222	28.37	14.19	0.25	3.14	0.005231624	273.37	10.89
400	32.89	16.44	0.29	2.72	0.00528573	273.50	10.88
440	47.21	23.61	0.41	1.92	0.007220776	209.56	10.881

622	56.02	28.01	0.49	1.64	0.008049808	195.10	10.87
						237.88	10.88
						23.79	

Table 4.4: Main characteristics of the XRD Bragg peaks of the Eu_2O_3 powder annealed at 700°C in air for 2h.

Plane(hkl)	**$2\theta_{(exp)}$ (deg)**	**$\theta_{(exp)}$ (deg)**	**$\theta_{(exp)}$(rad)**	**d_{exp} (Å)**	**FWHM(rad)**	**Average edge size (nm)**	**a_{exp}(Å)**
222	28.36	14.18	0.253	3.14	0.005030563	284.29	10.89
400	32.87	16.44	0.29	2.72	0.005322382	271.61	10.88
440	47.22	23.61	0.41	1.92	0.006248279	242.18	10.87
622	56.04	28.02	0.49	1.64	0.006943094	226.22	10.87
						256.08	10.88
						25.61	

The change in the Eu_2O_3 particles size after calcination could be the results of annealing, aggregation and sintering of small particles to form larger particles, which is in agreement with previous literature [1].

4.3 Optical characterization

4.3.1. Fourier Transform Infrared Spectroscopy (FT-IR)

FT-IR spectroscopy is an extreme useful tool used to identify the functional groups and the study of the vibrational motion of atom and molecules. In the FT-IR spectroscopy, a molecule only absorbs IR light of certain frequencies based on the characteristics of each molecule [17]. By studying the absorption spectrum, it is possible to identify the molecule type and the amount of molecules in the sample.

The FT-IR spectrums of the precursor $EuN_3O_9.5H_2O$, HB extract and samples annealed at different temperatures (300, 500 and 700°C) were obtained from KBr pallets using Thermo Scientific Nicolet Is10 FT-IR spectrophotometer at room temperature and were analysed with the origin as shown in the **Figures below** (**Fig 4.10- Fig 4.12**), in the spectral range of 4000-400 cm^{-1}.

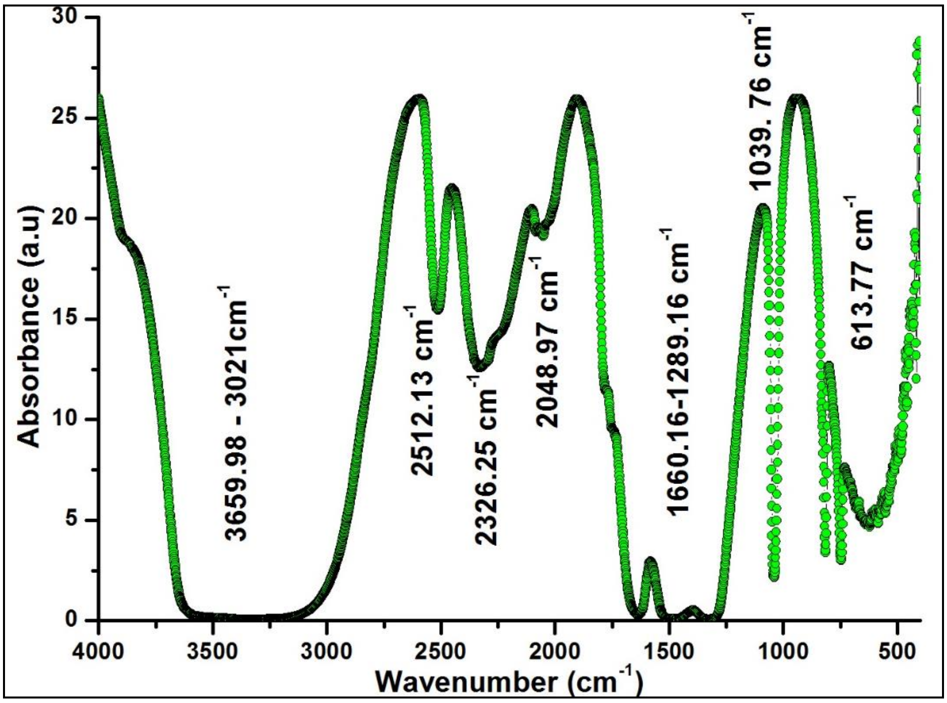

Figure 4.10: FT-IR absorption spectrum images of $EuN_3O_9.5H_2O$.

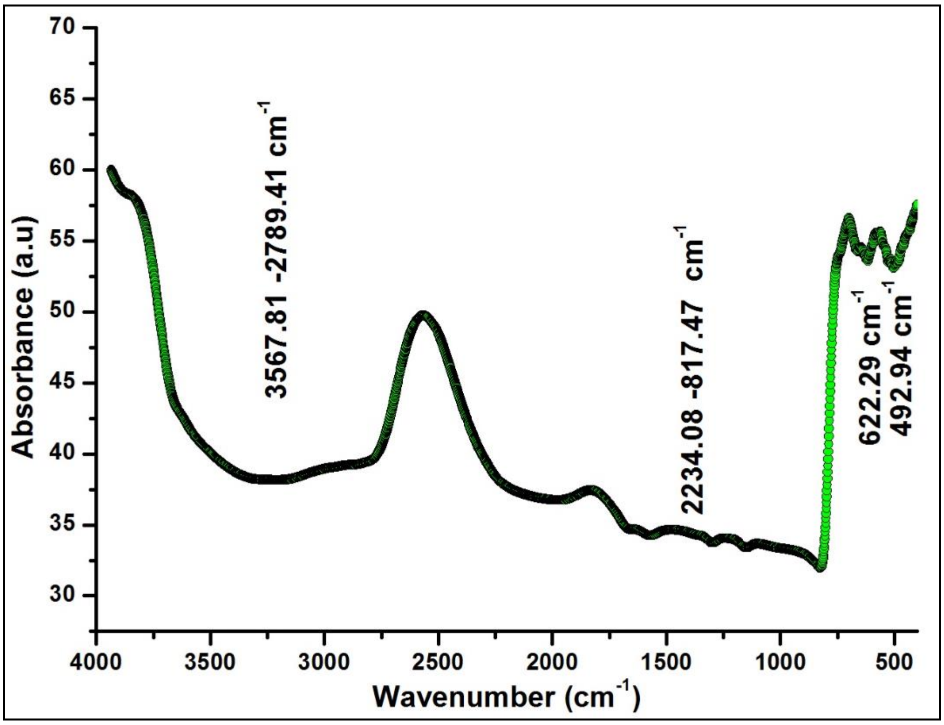

Figure 4.11: FT-IR absorption spectrum images of *hibiscus sabdariffa* flower extract.

The FT-IR spectra displayed in **Figure 4.10** shows the precursor and **Figure 4.11** the plant extract that was used to synthesize the Eu_2O_3 by mixing them together. Each spectrum shows several significant peaks. The obtained FT-IR absorption spectrum of $EuN_3O_9.5H_2O$ is also shown in **Fig 4.10** above. A hydrogen bonded O-H stretching was observed at 3659.9 to 30218 cm^{-1}, the stretching frequencies at 2512.13 -1289.16 cm^{-1} assigned to O-H, N-O, N = O stretching and N = O bending. Another sharp peak at 613.77 cm^{-1} corresponding to the bending O-H bond and N-O stretching.

The HB spectrum indicated in **Figure 4.11** exhibit a broad peak showing the stretching and bending characteristics at 2234.08 -817.47 cm^{-1} corresponding to stretching C-O, C = O and bending C-H, CH3, CH2, C-O-C, C-OH, C = C and OH. The weak bands observed at 622.29 and 492.94 cm^{-1} are characterized by the C-H, C = C and C-H bending modes. A broad peak observed at 3567.81-2789.41 cm^{-1} was created due to the adsorbed H_2O present on the other surface of the material and other bonds were identified which are characterized by the O-H, $COOCH_3$, COOH and C-H stretching modes. All these functional groups are found within the extract.

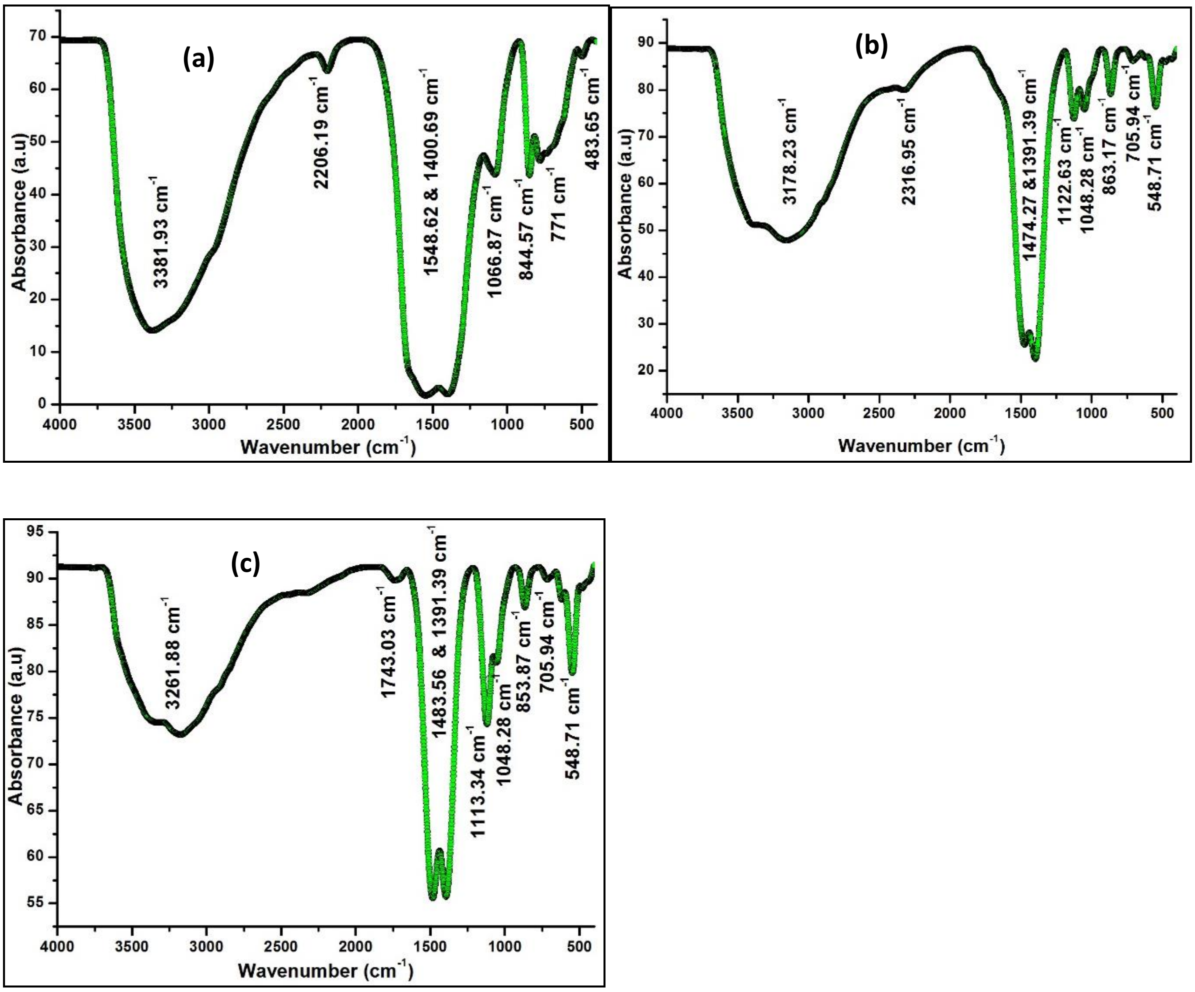

Figure 4.12: FT-IR absorption spectra of the Eu_2O_3 NPs annealed at different temperatures 300, 500 and 700°C for 2h.

In **Figure 4.12**, the spectra have several significant peaks recorded in the range from 4000-400 cm^{-1}. The FT-IR peaks show all the principal vibrational modes, which are in good agreement with the results reported by Kang et al. and Chaudhary et al. [2, 16]. The weak bands below 800 cm-1 are assigned to the bending of the aromatic carbon-hydrogen bond in the europium oxide NPs [2]. In **Figure 4.12 (a)**, the absorption broad peak at 3381.93 cm^{-1} is assigned to OH stretching vibrations of H_2O in the sample [2]. The peak from 1548.62 - 1400.69 cm^{-1} were commonly observed and ascribed to the asymmetric N-O stretching, N-H bending, NO_2 stretching and N-H stretching, respectively. The small peak at 1066.83 cm^{-1} corresponds to N-O symmetric stretching. The peak at 844.5 7 and 771 cm^{-1} were observed, which were attributed to the O-H bending vibration. Most of functional groups have decomposed because the samples were annealed at high temperatures to remove the unwanted gases/ nitrates in order to obtain pure Eu_2O_3 nanocrystals. The absorption at

483.65 cm^{-1} is produced by Eu_2O_3, which is the typical peak for the Eu bending showing the Eu_2O_3 NPs formation. The FT-IR spectrum displayed in **Figure 4.12 (b)** which was annealed at 500°C is the same as the spectrum in **Figure 4.12 (c)** that was annealed at 700°C, these results obtained exhibit significant peaks and they are in good agreement with the one reported on the previous literature by Kang et al. [2]. These spectra show several peaks, a broad peak in 3176.23 cm^{-1} was created due to the adsorbed (hydrated) H_2O present on the surface of the material. The characteristic stretching frequencies at 2316.95 cm^{-1} is assigned to C-H stretch band, 1483.56 -1391.39 cm^{-1} and 1048.28 cm^{-1} corresponds to the C = O and C-O stretches which shows the interaction of carboxylic acid with Eu(III) ions [15-16]. Since (Eu) is a heavy metal, its absorbance corresponds to lower frequencies and atoms coordinated to Eu also belong to lower frequencies of vibrations [14].

4.3.2 Raman Spectroscopy

The composition and crystalline structure were investigated by Raman spectrum collected from Eu_2O_3 nanopowder at a room temperature using nm Ar laser to excite the samples as shown in **Figure 4.13 below**. These different Raman spectra for rare-earth sesquioxides namely Eu_2O_3 NPs annealed at different temperatures 300 ^{o}C, 500 ^{o}C and 700^{o}C for 2 hours each, in the spectral range of 150-800 cm^{-1}.

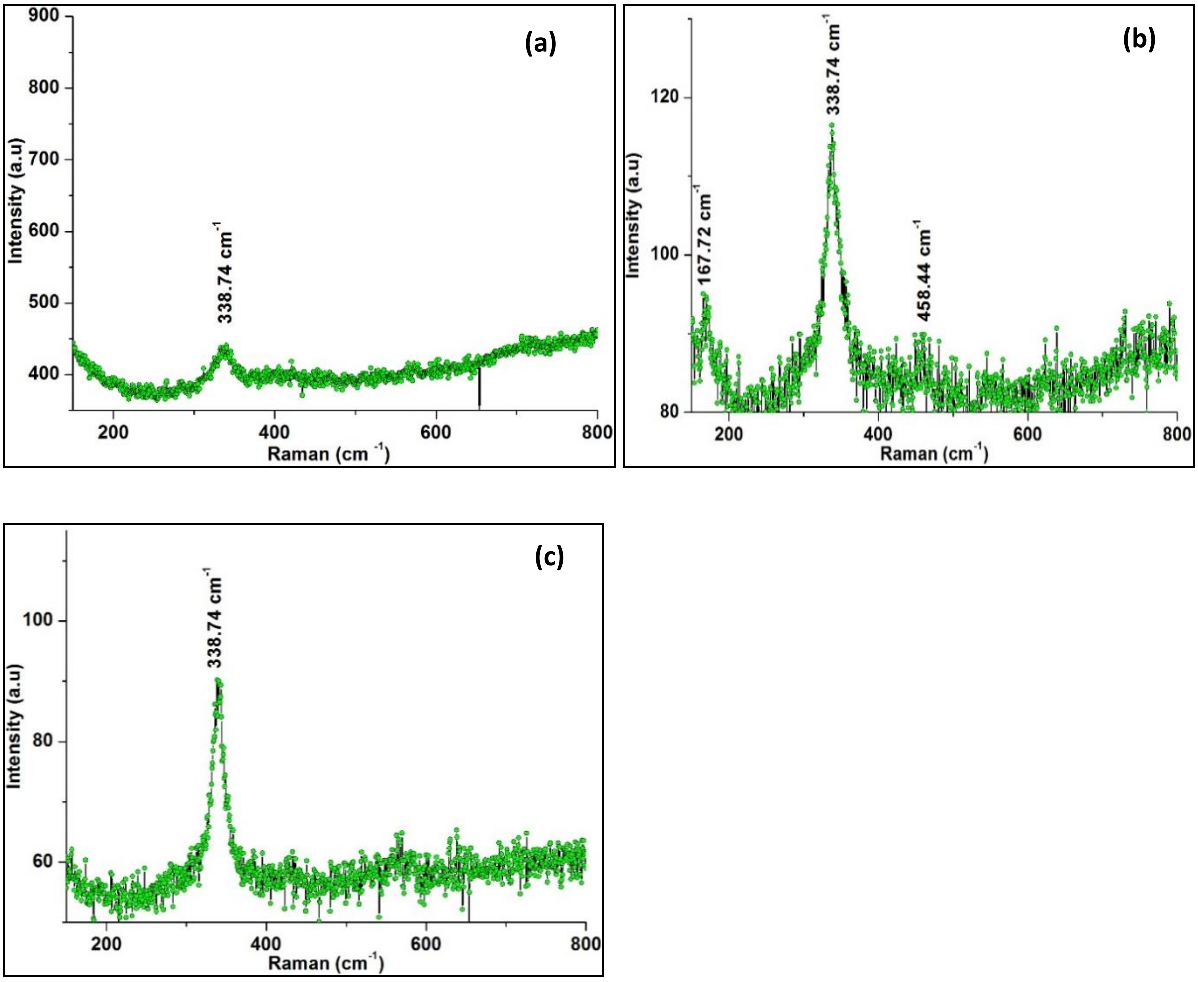

Figure 4.13: A Raman spectra for Eu_2O_3 annealed at (a) 300, (b) 500 & (c) 700 ^{o}C for 2 h.

The results of the Raman spectra for the obtained Eu_2O_3 are in good agreement with the results reported by Zeng et al., Tucker et al. and Dilawar et al. for Eu_2O_3. According to the group theory investigation, the C-type cubic Eu_2O_3 is estimated to have 22 Raman active modes namely 4Ag, 4Eg and 14Fg, respectively [1, 6, 11]. Experimentally one major peak was observed, centred at 338.74 cm^{-1} which is commonly in agreement with those reported in literature while other peaks are not yet available in literature. As shown in **Figure 4.13 (a)**, the Raman active mode is observed at 338.74 cm^{-1} commonly assigned to the symmetric Ag and degenerated Fg modes [5, 13], which are connected to the stretching vibrations of C_2-Octahedron (Eu_2-O).

In **Figure 4.13 (b)**, the Eu_2O_3 NPs annealed at 500 ^oC for 2 hours, showed a strong peak at 338.74 cm-1 corresponding to the symmetric Ag and degenerated Fg modes, which are connected to the stretching modes of the C_2-Octahedron (Eu2-O). The Eu_2O_3 NPs annealed at 700^oC shown in **Figure 4.13 (c)**, has the same Raman results as the above annealed at 300^oC and 500^oC. No other peaks were observed in these Raman spectra, which show that the nanopowder obtained is highly pure.

Due to the particle size effect of the nanoparticle, it has been suggested that small physical dimension of the scattering crystals lead to down of the first order Raman line [1, 6]. Such red shift may be attributed to size related effects with a decrease in the radius of nano solid. These results correspond well with the work reported by Tucker et al. and Dilawar et al. for Eu_2O_3 [6, 11].

4.3.3 Ultraviolet-visible spectroscopy (UV-Vis-NIR)

Further the generation of Eu_2O_3 NPs and their size modification were also identified by UV-visible analysis. Typically, the UV-Vis spectra of Eu_2O_3 nanoparticles was measured using Ocean Optics Maya2000 Pro Spectrometer that covers the range of ~165-1100 nm at a room temperature. The samples spectra are given in **Figure 4.14** below. The results are within the optical range of 200-800 nm and it has shown great absorbance characteristics of material which also corresponds to the literature reported.

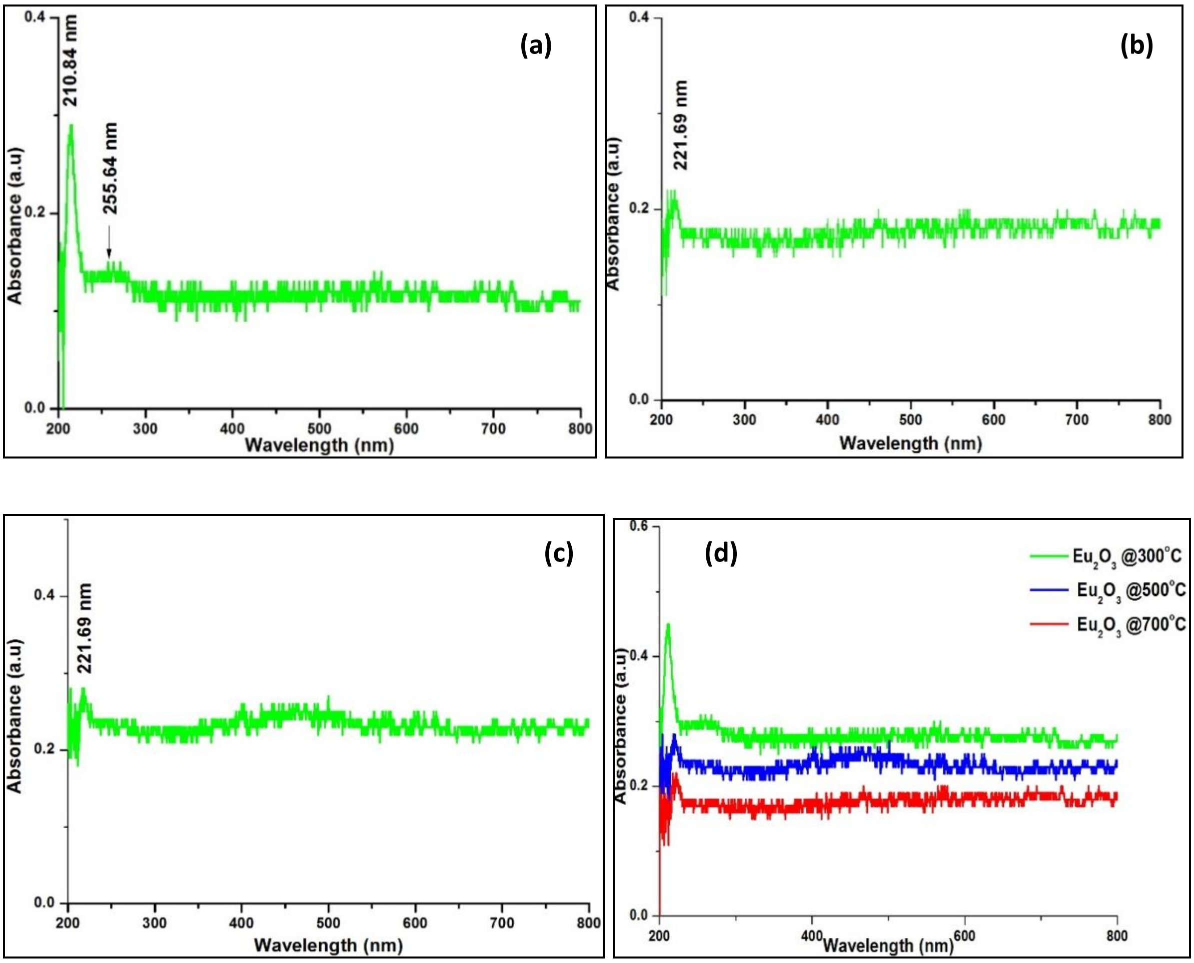

Figure 4.14: UV-Vis. Spectra of Eu_2O_3 NPs annealed at different tempertures 300, 500 & 700^{o}C.

The **Figure 4.14** above shows the UV-Vis spectra of Eu_2O_3 NPs annealed at different temperatures, 300, 500 and 700^{o}C. A strong absorption peak was observed below 300 nm, which corresponds well with the results reported by Kang et al. [2]. No other peaks were found above 300 nm, a strong sharp absorption peak which takes place at the ultraviolet (shorter wavelength) region 210.84 and 255.64 nm for sample that was annealed at 300°C in **Figure 4.14 (a)** and 221.69 nm corresponding to both 500 and 700°C with the electron transition of n to o* since Eu_2O_3 absorption occur in the ultraviolet region in **Figure 4.14 (b) & (c)**. **Figure 4.14 (d)** shows the UV- visible spectra of Eu_2O_3 nanoparticles at different temperatures, these results are similar to the ones reported by Chaudhary et al. [16], the UV-Vis spectra shifts towards higher wavelength with the increase of temperature, as shown in the spectra 500 and 700°C which slightly shift towards higher wavelength; in this case it moved from 210.84 to 221.69 nm which points towards the bigger particles and also cause the red shift in the absorption peak [16]. These peaks are assigned to 5d- 4f transitions of the Eu (III), the peak of the higher wavelength was created due to the O^{2-} -Eu^{3+} charge transfer state [2].

The optical band gap energy (Eg) of the prepared nanoparticles was further calculated using the following equation:

$$E = hc / \lambda \qquad 4.23$$

The E_g for 300°C is 5.89 eV, 500 & 700°C is 5.6 eV which corresponds to the one reported in the literature review. Moreover, the increase in the concentration of Eu $(NO_3)_3.5H_2O$ also causes the red shift in the absorption peak [16]. From the detailed spectral studies, it was observed that the variation of temperature on nanopowders have an influence on the optical properties of Eu_2O_3.

4.4 Conclusions

The as-prepared nanoscale amorphous Eu_2O_3 powder was annealed at 300 °C, 500 °C and 700°C for 2 hours under normal air conditions to obtain the crystallized Eu_2O_3 nanoparticles. The SEM, HRTEM and EDS analysis of Eu_2O_3 nanopowder illustrated that nanoparticles were successfully produced.

HRTEM results revealed that particles are formed by many aggregate agglomerated together, however the nanoparticles are non-uniformly dispersed.

XRD analysis of Eu_2O_3 nanoparticles illustrated the crystalline nature of the synthesized europium oxide nanoparticles. The results confirmed the characteristic body centered cubic (BCC) structure of Eu_2O_3 nanoparticles and is polycrystalline not amorphous.
The high purity of the synthesized Eu_2O_3 NPs was also revealed by Raman measurement, FT-IR, UV-Vis as well as PL.

The obtained FT-IR displayed significant peaks which revealed that the europium oxide produced is not pure due to some substituent peaks found after annealing. UV-Vis proved that Eu_2O_3 absorbs in a wide range of electromagnetic wave from ultraviolet region.

4.5 References

1. C. Zeng, K. Lou, X. Meng, Y. Zi-Qiao, Z. Ye, 'Synthesis of Porous Europium Oxide Particles for Photoelectrochemical Water Splitting', Electrochimica acta, vol. 165, 396-401 (2015).
2. J. Kang, Y. Jun, B. Min, Y. Sohn, 'Full characterization of Eu(OH)3 and Eu2O3 nanorods', Applied surface science , vol. 314, 158-165 (2014).
3. Y. Li, M. Ge, J. Li, J. Wang, H. Zhang, 'Synthesis of mesoporous Eu_2O_3 microspheres and Eu_2O_3 nanoparticle-wires as well as their optical properties', Society of chemistry, vol. 13, 637-641 (2011).
4. J. Feng, G. Shan, A. Maquieira, M.E. Koivumen, 'Fuctionalized Europium oxide nanoparticles used as fluorescent label in an immunoassay for atrazine', Analytical chemistry, vol. 75, 5282-5286 (2003).
5. A. Quesada, A. Campo, Jose F. Fernandez, 'Stabilization of cubic phase in dense Eu_2O_3 ceramics', Materials letter, vol. 157,77-80 (2015).
6. A. Diallo, B.M. Mothudi, E. manikandan, M. Maaza, 'Luminescent Eu_2O_3 nanocrystals by aspalatus linearis extract: structural and optical properties',Journal of nanophotonics, vol. 10(2), (2016).
7. W. Chen, A.G Joly, C.M Kowalchuk, J. Malm, Y. Huang, J Bovin, 'Structure,Luminescence and dynamics of Eu_2O_3 Nanoparticles in MCM-41', Journal of. physics and chemistry, vol. 106, 7034-7041 (2002).
8. Y. Castro, B. Julian, C. Boissiere, B. Viana, H. Amenitsch, D. Gross, C. Sanchez, 'Synthesis, characterization and optical properties of Eu_2O_3 mesoporous thin films', Nanotechnology, vol. 18, 7 (2007).
9. V.G Pol, R. Reisfeld, A. Gedanken, 'Sonochemical synthesis and optical properties of europium oxide nanolayer coated on titania', Chemical Material, vol. 14, 3920- 3924 (2002).
10. N. Dilawar, D. varandani, V.P Pandey, M. Kumar, S.M Shivaprasad, P.K. Sharma, A.K. Bandyopadhyay, 'Structural transition in nanostructures Eu_2O_3 under high pressures', Journal of nanoscience and nanotechnology, vol. 6, 105-113 (2006).
11. N. Dilawar, D. varandani, S. Mehrotra, B.V. Kumaraswamy, S.K Haldar, A.K. Bandyopadhyay, 'A raman spectroscopic study of C-type rare earth sesquioxides', Material characterization, vol. 59, 462-467 (2008).

12. L. Tucker, F. Karney, P. McMilan, S. Lin and L. lyring, ‘Raman and resonance raman spectroscopy of selected rare-earth sesquioxides’, Applied Spectroscopy, vol. 38, 857 (1984).

13. S. Kumar, R. Prakash, R.J Choudhary, D.M Phase, ‘Structural, XPS and magnetic studies of pulsed laser deposited Fe doped Eu_2O_3 thin films’, Material research bulletin, vol. 70 392-396 (2015).

14. P. Triny Trinh, ‘Luminescence studies of europium (III)-D-Glucosamine complexes in water’, Department of chemistry, San Jose State University.

15. K. Kattel, J. Park, W. Xu, H. Kim, G. Lee, ‘Water-soluble ultrasmall Eu_2O_3 nanoparticles as a fluorescence imaging agent: *in vitro* and *in vivo* studies’, Physicochemical and engineering aspects, vol. 394, 85-91 (2012).

16. S. Chaudhary, A. Umar, ‘Glycols functionalized fluorescent Eu_2O_3 nanoparticles effect on the structural and optical properties’, Journal of alloys and compounds, vol. 682 160-169 (2016).

17. K.K Babitha, A. Sreedevi, K.P. Priyanka, ‘Structural characterization and optical studies of CeO_2 nanoparticles synthesized by chemical precipitation’, Journal of pure and applied physics, vol. 53, 596-603 (2015).

18. Q. Chen, S. Zeng, ‘Study on preparation and fluorescence characteristics of coordinated Eu_2O_3 /polymer hybrid films’, Applied surface science, vol. 254, 5304-5313 (2008).

CHAPTER FIVE: APPLICATION OF Eu_2O_3 NPs

5.1. Photoluminescence (PL) properties

Rare earth oxides have been the focus of many structural, electrical and optical studies due to their major importance in the production of phosphors, photonics sensors and solid state opto-electronics, as well as their pivotal role in the telecommunications, and the new generation of photo-conversion-based solar cells devices [1-3]. Among them, europium oxide (Eu_2O_3) is one of the most attractive rare earth oxides shown recently to exhibit improved luminescence/ fluorescence responses, as was demonstrated on Tb (III)-doped and NdF3/SiO_2 [4-7]. Eu_2O_3 has several applications including red or blue phosphor in television, fluorescent lamps, production of fluorescent glass, anti-counterfeiting phosphors in euro banknotes and also known as a great neutron absorber which is used in nuclear control rods [8-9].

Since Eu_2O_3's major emission band is centered at 612 nm due to its well-defined transition within the 4d and 4f electrons shell [14], therefore its usage in phosphors and luminescent devices is paramount [13-14]. Eu_2O_3 is one of the most important oxide phosphors [14] and Eu^{3+} is particularly interesting because of its major emission band [17]. For this reason Eu^{3+} ion has been investigated thoroughly as an excellent luminescence red emitting activator ion in many host lattice by the transition of $^5D_0 \rightarrow {}^7F_2$ [14, 17, 19]. In general, oxide phosphors are suited for applications such as low voltage cathodoluminescent devices because they show improve stability in high vacuum environment as well as lower contamination gas emission [18]. Due to its good fluorescence properties, the photo luminescence experiment was conducted.

The PL properties of Eu_2O_3 NPs was investigated under ambient temperature within the spectral range of 350-800 nm, the emission spectra was taken at a fixed excitation wavelength of λ_{exc}= 300 nm line of an Hg lamp on Fluorolog-Horiba unit. The results indicated in **Figure 5.1** were obtained.

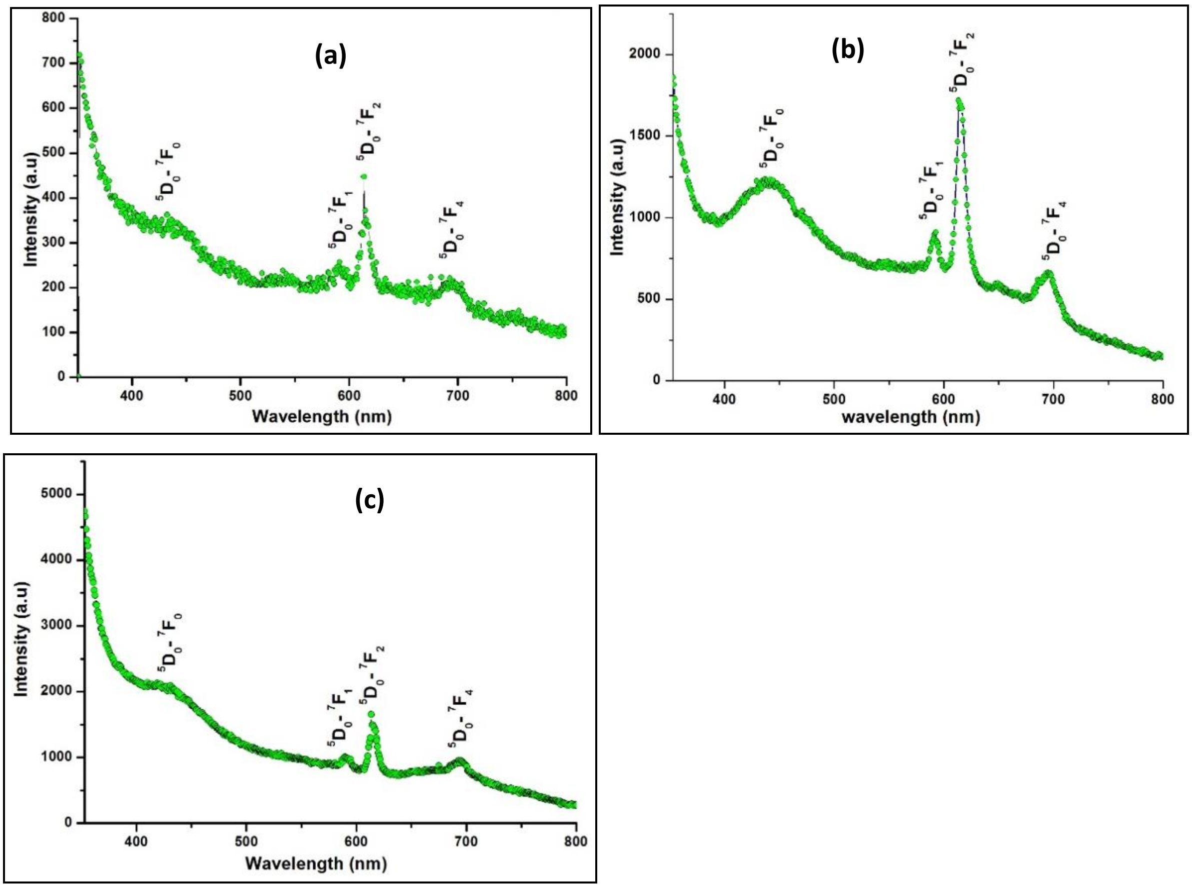

Figure 5.1: Room temperature photoluminescence spectra of Eu_2O_3 NPs annealed at 300 °C **(a)**, 500 °C **(b)** & 700°C **(c)** with the excitation wavelength of 300 nm.

Figure 5.1 exhibits the room temperature emission spectra of Eu_2O_3 NPs annealed at 300, 500 and 700°C. In **Figure 5.1 (a)**, four dominant emission peaks were observed and were centred at 438.01, 591.94, 612.85 and 694.95 nm for nanopowder annealed at 300°C. **Figure 5.1 (a)** and **(b)** are more or less the same. More accurately the emission peaks are centred at 440.31, 591.73, 614.93 and 694.71 nm. There is a sharp intense peak centred at 614.93 nm which could be due to the primary contribution of $^5D_0 \rightarrow ^7F_2$ transition of Eu(III) respectively. The other emission peaks observed above 580 nm were attributed to $^5D_0 \rightarrow ^7F_j$ = 0, 1, 2, 3 which associated $^5D_0 \rightarrow ^7F_0$, $^5D_0 \rightarrow ^7F_1$, $^5D_0 \rightarrow ^7F_2$ and $^5D_0 \rightarrow ^7F_4$ from the energy level diagram at optical transition within Eu^{3+} ion in the **Figure 2.2** that was mentioned in chapter

2. The dominant emission peak $^5D_0 \rightarrow ^7F_2$ observed at 614.93 nm confirms the cubic nature of the biosynthesized Eu_2O_3 nanoparticles [12, 13], and it is also an interesting peak corresponding to a hypersensitive forced electric dipole transition. Since the peaks are broader they confirm the nanoscale size and low dimensional nanocrystals of Eu_2O_3 [13]. These results are consistent with the previous results reported by Diallo et al. [13]. As the temperature is increased, the intensity also increases and the wavelength is red shifted.

The $^5D_0 \rightarrow ^7F_2$ transition become much stronger than the other peaks which is consistent with the previous results/ studies [11, 13-15].

The band gap energy (Eg) for different wavelength was calculated and the value found was within 2-3 eV which falls within the expected range of Eu_2O_3 NPs. As the wavelength increases the energy decreases and these spectral shifts correspond to the effect of size of the prepared nanoparticles. These emission wavelengths correspond to a red colour.

The calculated energy spectra for different wavelengths are displayed in **table 5.1** below; the table summarizes results obtained from PL. In this project it was found that Eu_2O_3 NPs has a good fluorescent/ photoluminescence properties.

Table 5.1: The PL peak, wavelength and the calculated energies of the Eu_2O_3 annealed at **(a)** 300, **(b)** 500 and **(c)** 700°C.

(a)

Peak	**Peak position (nm)**	**Energy (eV)**
1	483.01	2.833
2	591.94	2.096
3	612.85	2.025
4	694.95	1.785

(b)

Peak	**Peak position (nm)**	**Energy (eV)**
1	440.31	2.818
2	591.73	2.096
3	614.93	2.018
4	694.7	1.786

(c)

Peak	Peak position (nm)	Energy (eV)
1	426.48	2.909
2	590.57	2.101
3	614.93	2.018
4	694.61	1.768

Our PL spectra shows consistent results with those observed by other research groups [16]. Since the PL emission show that Eu_2O_3 emits intense red light under visible radiation.

The photoluminescent analysis of Eu_2O_3 nanoparticles indicated in **Figure 5.1**, confirms that Eu_2O_3 is a good luminescent material shown by its extremely sharp emission band with high luminescent efficiency. The PL peak position at 614.93 nm band is assigned to the Eu^{3+} transition $^5D_0 \rightarrow {}^7F_2$ emitting intense red light. It was also indicated that as the temperature increases from 300°C to 700°C, a strong Eu^{3+}photoluminescence take place indicating high color purity. These results are in correspondence with the one reported by Chen et al, [14]. Finally, due to the strong red luminescence of Eu^{3+}, Eu_2O_3 proves to be a good candidate to be used as phosphors and is represented as an efficient material with potential applications. Since the luminescent can be further improved by doping, an experiment for doping would be performed in near future.

In summary the PL results obtained exhibit that Eu_2O_3 is emitting better in the range of 350 to 800 nm and the emission peaks were attributed to the $^5D_o \rightarrow {}^7F_j$ transition. A strong fluorescence in the red region was observed due to their particle size. As the temperature was increased the size of NPs was increasing; at 300 °C the average particle size was 14.71 nm, 500 °C was 23.79 and at 700 °C was 25.61 nm. It was observed that a biosynthesized cubic Eu_2O_3 nanocrystal is an efficient luminescence material due to a very good luminescent response with potential application as red phosphors.

5.2. References

1. A. Dakhel, 'DC electrical measurements on gadolinium-erbium oxide films prepared on Si(100) substrates', Applied physics, vol. 6, 32-36 (2006).
2. M. Jayraj, C. Vallabhan, 'Dielectric and optical properties of europium oxide films', Thin solid films, vol. 177, 59- 67 (1989).
3. P. Meena, 'Conduction studies on europium oxide thin films', Journal of solid state physics, vol. 177, 207-214 (1993).
4. G. L. Wong, 'Functionalized europium nanorods for invitro imaging', Inorganic chemistry, vol. 47, 5190-5196 (2008)
5. L. Li, 'Surface modification of hydroxyapatite nanocrystallite by small amount of terbium provides a biocompatible fluorescent probe', Journal of physics and chemistry, vol. 112, 12219-12224 (2008).
6. R. M. Petoral, J' Synthesis and characterization of Tb3+ - doped Gd2O3 nanocrystals: a bifunctional material with combined fluorescent labelling and MRI contrast agent properties', Journal of physics and chemistry, vol. 113, 6913-6920 (2009)
7. X. F. Yu, 'Highly efficient fluorescence of NdF3/SiO2 core/ shell nanoparticles and the applications for in vivo NIR detection', Advanced material, vol. 20, 4118-4123 (2008)
8. D. Lee, J. Seo, L. Valladares, O.A. Quispe, H.W. Barnes, 'Magnetic and structural properties of yellow europium oxide compound and $Eu(OH)_3$', Journal of solid state chemistry, vol. 228, 141-145 (2015).
9. L. Tucker, F. Karney, P. McMilan, S. Lin, L. lyring, 'Raman and resonance raman spectroscopy of selected rare-earth sesquioxides', Applied Spectroscopy, vol. 38, 857 (1984).
10. C. Zeng, K. Lou, X. Meng, Y. Zi-Qiao, Z. Ye, 'Synthesis of Porous Europium Oxide Particles for Photoelectrochemical Water Splitting', Electrochimica acta, vol. 165, 396-401 (2015).
11. J. Kang, Y. Jun, B. Min, Y. Sohn, 'Full characterization of Eu(OH)3 and Eu2O3 nanorods', Applied surface science , vol. 314, 158-165 (2014).
12. J. Feng, G. Shan, A. Maquieira, M.E. Koivumen, 'Fuctionalized Europium oxide nanoparticles used as fluorescent label in an immunoassay for atrazine', Analytical chemistry, vol. 75, 5282-5286 (2003).

13. A. Diallo, B.M. Mothudi, E. manikandan, M. Maaza, 'Luminescent Eu_2O_3 nanocrystals by aspalatus linearis extract: structural and optical properties',Journal of nanophotonics, vol. 10(2), (2016).

14. W. Chen, A.G Joly, C.M Kowalchuk, J. Malm, Y. Huang, J Bovin, 'Structure,Luminescence and dynamics of Eu_2O_3 Nanoparticles in MCM-41', Journal of. physics and chemistry, vol. 106, 7034-7041 (2002).

15. P. Triny Trinh, 'Luminescence studies of europium (III)-D-Glucosamine complexes in water', Department of chemistry, San Jose State University.

16. K. Kattel, J. Park, W. Xu, H. Kim, G. Lee, 'Water-soluble ultrasmall Eu_2O_3 nanoparticles as a fluorescence imaging agent: *in vitro* and *in vivo* studies', Physicochemical and engineering aspects, vol. 394, 85-91 (2012

17. Q. Chen, S. Zeng, 'Study on preparation and fluorescence characteristics of coordinated Eu_2O_3 /polymer hybrid films', Applied surface science, vol. 254, 5304-5313 (2008).

18. S.A. Lourenco, N.O. Dantas, E.O. Serqueria, 'Eu3+ photoluminescence enhancement due to thermal energy transfer in Eu_2O_3-doped SiO2-B2O3-PbO2 glasses system', Journal of luminescence, vol. 131, 850-855 (2011).

19. N. Omar, Y. Fen, K. Maroti,'Structural and optical properties of Eu3+ activated low cost zinc soda lime silica glasses', Results in physics, (2016).

CHAPTER SIX: CONCLUSIONS

6.1. Overall Conclusion

Nanotechnology and nanoscience are still growing rapidly in terms of research due to the properties they have exhibited and their extensive applications. Metal oxide nanoparticles play a very important role in many areas such as physics, chemistry and material sciences. The current research focuses on the material synthesis and their promising properties achieved via the green physical-chemistry process. Eu_2O_3 NPs were successfully prepared by an environmentally friendly process using natural extract of *hibiscus sabdariffa* flowers, that acted as both chelating and reducing chemical agent. A thermal annealing at different temperatures (300, 500 and 700^{o}C) resulted in highly crystallized phase Eu_2O_3 NPs as confirmed by SEM, HRTEM, EDS, XRD, FT-IR, Raman, UV-Vis-NIR and PL measurements.

SEM and HRTEM analysis of Eu_2O_3 nanoparticles revealed various shapes of Eu_2O_3 NPs produced but mostly are spherical like and it was observed from SAED that Eu_2O_3 NPs are polycrystalline with body –centred cubic crystal structure. However, the nanoparticles are non-uniformly dispersed. Since this was synthesized for the first time, further investigation on the effect of concentration, pH and solvent should be conducted in the future.

XRD analysis of Eu_2O_3 nanoparticles revealed the highly crystalline nature of the synthesized Eu_2O_3 nanoparticles. These results confirmed the characteristics of the body centred cubic (bcc) structure of europium (III) oxide nanoparticles. The size of nanoparticles increases and the temperature increases and was calculated using Debye-Sherrer formula, the grain size ranging from 10-25 nm. It was observed that calcination improves the crystallinity of the samples and also the prepared Eu_2O_3 nanoparticles revealed that other material/ elements from the natural extract and precursor decomposes as at high temperatures. These results were confirmed by the FT-IR spectroscopy.

The EDS, FT-IR and Raman analysis revealed that Eu_2O_3 nanopowder samples are of a significant chemical purity. Pure phase of Eu_2O_3 was not achieved as reflected from the FT-IR investigation; the spectra is not smooth and still shows other peaks (substituents) existing within the material produced. The UV-Vis investigation exhibited high absorbance of Eu_2O_3 NPs. The PL measurements proved that nano-scaled Eu_2O_3 material exhibit improved fluorescence properties, as the major emission band was centred at about 614.93 nm due to its well-defined transition within 4d and 4f electron shell which confirm its potential usage in phosphors and luminescence devices. Therefore it was shown that nanoscaled Eu_2O_3 material specifically exhibit improved luminescent/ fluorescent responses.

The current biosynthesis of such small crystalline Eu_2O_3 demonstrated for the first time via *hibiscus sabdariffa*, confirmed the possibility of using this cost-effective green process in the design of high quality multi-oxide and simple rare earth compounds at nano-scale size.